Green Chemistry

Cutting-edge research for a greener sustainable future

ROYAL SOCIETY
OF **CHEMISTRY**

CRITICAL REVIEW
Chang-Gu Lee, Seitkhan Azat, Jechan Lee *et al.*
Mining waste as heterogeneous catalysts

25 YEARS ANNIVERSARY

Check for updates

Mining waste as heterogeneous catalysts

Soo Lim Kim,†[a] Heejin Yang,†[b] Seonho Lee,[a] Si-Kyung Cho,[c] Chang-Gu Lee, [iD] *[b,d] Seitkhan Azat*[e] and Jechan Lee [iD] *[a,f]

Mining activities generate significant waste that poses serious environmental challenges, emphasizing the urgent need for effective waste management strategies. Mining waste, such as tailings, pyritic materials, ore residues, and metallurgical by-products, is rich in metals and metal oxides (e.g., Mg, Fe, and Al species) that can serve as catalytic active sites or supports. This intrinsic property highlights its potential for application as heterogeneous catalysts. In recent years, there has been growing interest in utilizing mining waste for catalytic applications, sparking preliminary studies that explore its catalytic capacities and mechanistic roles across various processes. This review consolidates recent advancements in employing mining waste as catalysts, focusing on their characterization, preparation methods, and catalytic performance in diverse reactions. These include dry and steam reforming, wastewater treatment processes (e.g., Fenton, photo-Fenton, peroxymonosulfate activation, electrochemical methods, and ozonation), environmental remediation (e.g., denitrification, carbon monoxide oxidation, and carbon dioxide reduction), and other chemical transformations (e.g., esterification, acetylation, and hydrodeoxygenation). Furthermore, the review discusses key challenges and critical considerations for advancing research in mining waste-based catalysts.

Green foundation

Green chemistry is a set of practices that reduce or eliminate the use of hazardous chemicals in order to minimize pollution. Green chemistry can be applied to mining waste to reduce the environmental impact of the mining and relevant industries via the following points: use heterogeneous catalysts to minimize waste streams in chemical reactions; recycle mining waste to create new materials; use residual by-products as raw materials to create value-added products. In this regard, this review proposes the re-use of mining waste, one of the world's most generated types of waste, as heterogeneous catalysts. It not only evaluates the type and characteristics of mining waste that can be used for catalysts and relevant catalyst preparation methods, but also investigates applications of mining waste-derived catalysts for various chemical reactions (e.g., syngas/H_2 production, wastewater treatment, environmental remediation, and various chemical conversion reactions).

1. Introduction

Mining operations produce vast amounts of waste during the extraction and processing of mineral resources, including topsoil overburden, waste rock, and tailings.[1] Appropriate

[a]Department of Global Smart City, Sungkyunkwan University, Suwon 16419, South Korea. E-mail: jechanlee@skku.edu

[b]Department of Energy Systems Research, Ajou University, Suwon 16499, South Korea

[c]Department of Biological and Environmental Science, Dongguk University, Goyang 10326, South Korea

[d]Department of Environmental and Safety Engineering, Ajou University, Suwon 16499, South Korea. E-mail: changgu@ajou.ac.kr

[e]Laboratory of Engineering Profile, Satbayev University, Almaty 050013, Kazakhstan. E-mail: s.azat@satbayev.university

[f]School of Civil, Architectural Engineering, and Landscape Architecture, Sungkyunkwan University, Suwon 16419, South Korea

† Co-first authors.

management of these waste streams is critical for mitigating their harmful effects on the environment and human health.[2] Mining waste is among the largest global waste streams, with billions of tons generated annually.[3] For example, a survey of 107 mining companies estimated the global annual production of tailings to be approximately 13 billion tons, with at least 44.5×10^9 m^3 of tailings stored at mine sites.[4] The global mining waste management market size was estimated to be approximately 183 billion tons in 2023 and is projected to increase to ≈232 billion tons by 2032 at a compound annual growth rate of 2.7% between 2024 and 2032.[5] The mining waste generated is often sent for recovery or neutralization for disposal in dedicated landfills that involve ground storage in neutralization tanks.[6] However, it still raises the possibility of leakage into the ground, posing a threat to the surrounding area, and pretreatment for disposal generates additional waste.[7] Moreover, current mining waste storage and treatment facilities are unprofitable,[8] which might result in the disas-

trous spread of contaminants and increase mine waste-associated impacts.[9] Consequently, there has been a surge in suitable mining waste treatment strategies.

Mining waste may contain hazardous substances; however, not all mining waste poses environmental harm. In fact, a significant portion of mining waste holds valuable and reusable resources. For example, mining waste has been repurposed as construction materials[10–16] and geopolymer[17–20] products, offering sustainable alternatives in these industries. Furthermore, recoverable metals and minerals can often be extracted from mining waste, adding economic and environmental value.[21–23] Some types of mining waste also contain metals and metal oxides that exhibit catalytic properties, making them suitable for use as catalysts in various chemical reactions. Although several studies have explored the use of mining waste in catalytic reactions, much of this research is fragmented and lacks a comprehensive framework. This gap highlights the need for a systematic review to thoroughly evaluate the potential of mining waste as catalytic materials. Accordingly, this review is organized to examine the diverse applications of mining waste as catalysts by consolidating and analyzing findings from recent studies. Specifically, section 2 classifies the types and characteristics of mining waste that can be used as catalysts. Section 3 introduces and compares the methods used to prepare mining waste-derived catalysts, examines their properties, and discusses their performance in various reactions. Section 4 identifies the current limitations of mining waste-based chemical processes and offers research recommendations to overcome these challenges. This study contributes novel insights in comparison with earlier reviews,[24–30] as summarized in Table 1.

2. Mining waste as raw materials for heterogeneous catalysts

Various types of mining wastes were used for heterogeneous catalyst preparation (Fig. 1 and Table 2). The mines presented in Fig. 1 produce bauxite, iron, flint kaolin, pumice, rare earth

elements, *etc.*,[31] which also generate mining waste consisting of a range of metals and metal oxides (Table 2). Most mining waste remains unused as a resource, leading to environmental and health issues. For example, the metallic substances in abandoned mining waste can cause environmental pollution through various pathways such as the leaching of heavy metals from mining and smelting and non-point source pollution from rainfall and atmospheric transport. This pollution has serious impacts on the environment and human health.[32] Given that green chemistry is defined as the '*Design of chemical products and processes that reduce or eliminate the use or generation of hazardous substances*', appropriate reuse of mining waste as heterogeneous catalysts substantially contributes to achieving green chemistry principles in the field of chemical production processes.

The composition of mining waste is closely related to the type of mined materials and resources as well as the mining methods employed.[59] Table 2 provides a summary of the compositions of several mining waste samples that have been utilized as heterogeneous catalysts in different chemical reactions. Mining waste typically contains a mixture of metal and metal oxide species, with major components including Fe (Fe_2O_3), Mg (MgO), Al (Al_2O_3), and Si (SiO_2). These species are well-recognized as catalytic active sites or catalyst supports for numerous chemical reactions.[60–66] Consequently, mining waste holds significant potential for use as heterogeneous catalysts. However, mining waste often contains impurities that may hinder its catalytic performance. For instance, while commercial kaolin consists primarily of aluminosilicate, kaolin mining waste also includes Fe and Ti impurities, which reduce kaolin brightness and decrease its crystallinity.[67,68] Depending on the type of reaction, these impurities can significantly impair catalytic activity. As a result, effective pre- and post-treatment processes are often required to remove impurities, enhance crystallinity, and improve the material's properties as a solid support.[69] In sections 3–5, a range of heterogeneous catalysts derived from mining waste and their applications in various chemical reactions are explored in detail.

Table 1 Comparison of earlier reviews and this review on the reuse of mining waste

Review	Way to reuse mining waste	Focus on
Lim and Alorro[24]	Recovery of metal and mineral resources	• Technospheric mining • Metal recovery techniques
Vitti and Arnold[25]	Recovery of metal and mineral resources	• Extraction techniques for mineral & metal recovery mine tailings
Sarker *et al.*[26]	Recovery of metal and mineral resources	• Characteristics of precious metals found in mining waste • Precious metal recovery techniques
Abbadi *et al.*[27]	Recovery of metal and mineral resources	• Processes for rare Earth metal recovery
Xiaolong *et al.*[28]	Synthesis of geopolymers	• Methods for producing geopolymers from mining waste • Pre-treatment of mining waste to enhance geopolymer reactivity
Carmignano *et al.*[29]	Preparation of construction materials	• Applications relying solely on iron ore tailings • Limited discussion on catalyst preparation and applications
Barraza *et al.*[30]	Synthesis of nanomaterials	• Tailing reprocessing for nanomaterial synthesis • Recovery of metal and metal oxide nanoparticles from mining tailings • Application of the tailing-derived nanomaterials
This review	Use as heterogeneous catalysts for various reactions	• Components of mining waste with regard to catalytic activity • Methods to prepare catalysts from different types of mining waste • Chemical reactions facilitated by mining waste-derived catalysts

Fig. 1 Origins of various mining wastes used for heterogeneous catalyst preparation.

Table 2 Compositions of various mining wastes used for heterogeneous catalyst preparation

Mining waste	Components (content, %)	Ref.
Waste ore	• Fe_3O_4, Fe_2O_3, Co_2O_3, Co_3O_4, CuO, SiO_2, MgO	33
Iron mining waste	• Fe_2O_3 (25), Fe_3O_4, FeOOH, FeO, CeO_2 (8), Ce_2O_3, P_2O_3, SiO_2, Al_2O_3, La_2O_3, CaO, BaO, TiO_2, MnO, ZnO, $Al(OH)_3$, MgO, $MgFeAlO_4$, $MgFe_2O_4$, $AlFe_2O_4$	34, 35, 36, 37 and 38
Magnetic mining waste	• Fe_2O_3 (73.72–75.85), TiO_2 (9.48–10.09), P_2O_5 (3.58–3.92), SiO_2 (2.92–6.3), CaO (2.18–2.57), MgO (0.85–2.12), MnO (0.91), Al_2O_3 (0.53–0.78), K_2O (<0.05), Na_2O (<0.05)	39 and 40
Tailings and slag originating from Serifos Island (Cyclades, Greece)	• FeO (97.42), MgO (0.67), Al_2O_3 (0.37), SiO_2 (0.23), MnO (0.12)	41
Slag residue from metal mining	• $MgFe_2O_4$, $MgFeAlO_4$, Fe_3O_4, Al_2FeO_4, NiO, MgO, MgO_2	42 and 43
Amethyst mining reject	• SiO_2 (37.48), Fe_2O_3 (24.36), Al_2O_3 (13.56), CaO (12.44), TiO_2 (6.17), MgO (2.08), K_2O (1.23), P_2O_5 (1.18), SO_3 (0.46), MnO (0.37), others (0.67)	44
Bauxite mining waste	• α-Fe_2O_3 & α-FeO(OH) (41), Al_2O_3 (17), SiO_2 (10), TiO_2 (9), CaO (9), Na_2O (5)	45 and 46
Basalt mine tailings	• SiO_2 (41.88), Fe_2O_3 (22.97), CaO (11.84), Al_2O_3 (11.74)	47
Ilmenite metallurgical residue	• Fe (31.26), Mg (17.49), Al (5.35), Ca (1.07), Mn (1.01), V (0.90), Ti (0.60), Cr (0.51), Na (0.17), Si (0.08), K (0.02), P (0.004), Zr (0.01), Zn (0.01)	48
Pyritic waste	• SiO_2 (8.44), Al_2O_3 (2.55), CaO (0.12), K_2O (0.19), Cr_2O_3 (0.04)	49
Pumice mining waste	• SiO_2 (48.069), Al_2O_3 (8.275), K_2O (4.312), Fe_2O_3 (1.591), Na_2O (1.207), CaO (0.782), MgO (0.438), MnO (0.253), ZrO_2 (0.052), P_2O_5 (0.044)	50
Rare Earth tailings	• Fe_2O_3 (27.67), CaO (27.2), SiO_2 (11.86), MgO (3.31), CeO_2 (3.01), MnO (1.96), Al_2O_3 (1.46), La_2O_3 (1.44), Nd_2O_3 (1.10), TiO_2 (1), F (8.92), CaF_2, $Ce(CO_3)F$	51, 52 and 53
Kaolin waste	• SiO_2 (39.43–42.30), Al_2O_3 (38.29–39.92), TiO_2 (3.20–3.25), Fe_2O_3 (2.92–3.4)	54 and 55
Coal gangue	• SiO_2 (8.38–58.3), Al_2O_3 (9.11–20.8), Fe_2O_3 (1.01–10), SO_3 (0.05–3.97), K_2O (0.05–4.75), MgO (0.98–2.11), CaO (0.02–1.59), TiO_2 (0.51–0.98), Na_2O (0.81), ZrO_2 (0.01)	56, 57 and 58

3. Syngas and H_2 production using mining waste-derived catalysts

3.1. Mining waste catalysts prepared for producing syngas and H_2

As seen in section 2, mining waste can contain various metal oxides. Many of them are used either as catalyst supports or as catalytic active sites. When mining waste is used as the support to prepare catalysts for syngas or H_2 production (sections 4.1 and 4.2), Ni is loaded on mining waste in most studies.[34,42,48,56,70–73] Metals other than Ni, including Ru and Rh, have very rarely been tested for the reactions.[74] Impregnation-based methods were most widely used to prepare mining waste-supported Ni catalysts using Ni nitrate (e.g., $Ni(NO_3)_2 \cdot 6H_2O$) as the Ni precursor. To make a pelletized

Table 3 Mining waste-supported Ni catalysts used for syngas and H_2 production

Entry	Mining waste support (major components)	Properties							
		Ni loading (%)	Surface area ($m^2 g^{-1}$)	Total pore volume ($cm^3 g^{-1}$)	Average pore diameter (nm)	Average particle size (nm)	Ni spinel crystallite size (nm)	Surface Ni sites	Ref.
1	Ilmenite metallurgical residue (Fe, Mg, Al oxides)	13.9	3.94	0.019	—	168	—	—	44
2	Metallurgical residue	A form of powder	4.1	—	—	—	29.4	—	48
3	Metallurgical residue	A form of pellet (25% clay)	0.4	—	—	—	56	—	48
4	Iron-rich mining residue (Fe, Mg, Ce oxides)	5–13	2.91–2.87	0.0134–0.0132	18.2–17.7	—	3.38–3.41	—	45
5	Mining residue	13	2.77	0.0177	—	—	—	—	49
6	Slag residue from metal mining (Mg–Fe oxides)	10	4.86	0.023	7.87	—	—	565.8 cc g^{-1}	46
7	Agglomerates of metallurgical residue	12.5	10.3	—	—	—	—	—	50
8	Agglomerates of metallurgical residue	5	9.9	0.13	52.8	604.2	—	Ni dispersion = 0.17%	51
9	Coal gangue (SiO_2, Al_2O_3, Fe_2O_3)	15	5.38	0.033	17.86	—	—	—	47

form of a Ni/metallurgical residue catalyst, clay was mixed with the Ni precursor prior to impregnation.[70] The form of Ni catalyst (powder or pellet) could affect the catalytic activity for dry reforming, as discussed in the following subsection.

Table 3 shows the physicochemical properties of different Ni catalysts supported on mining waste. The mining waste-supported Ni catalysts tended to have lower surface areas (up to 10 $m^2 g^{-1}$), porosity (up to 0.03 $cm^3 g^{-1}$), and metal dispersion (<1%) than typical Ni catalysts supported on pure Al_2O_3 or SiO_2 most likely due to the co-existence of different oxides, minerals, and impurities in mining waste (Table 2). The Ni loading on mining waste was found to be an important factor affecting the catalyst's physicochemical properties. For example, an increase in Ni loading on the Ni catalyst supported by iron-rich mining residue resulted in a reduction of the catalyst's surface area, pore volume, and pore size.[34] However, the Ni loading did not significantly affect the crystal size of Ni spinel ($NiFe_2O_4$) present on the catalyst.

3.2. Syngas production

Synthesis gas (syngas) is a mixture primarily composed of H_2 and CO in varying ratios. It serves as a critical intermediate for the production of ammonia,[75] methanol,[76] and hydrocarbon fuels.[77] Syngas is also combustible, making it suitable for direct use as a fuel.[78,79] Several studies have investigated syngas production using mining waste-derived catalysts *via* dry reforming and steam reforming, as summarized in Table 4 (entries 1–6).

3.2.1. Dry reforming. Dry reforming is the production of syngas by the reaction between a feedstock (*e.g.*, CH_4 and C_2H_4) and CO_2. Dry reforming of CH_4 ($CH_4 + CO_2 \rightarrow 2CO + 2H_2$, $\Delta H_{298}^{\circ} = 247 \text{ kJ mol}^{-1}$) is a highly endothermic catalytic reaction that converts CH_4 and CO_2 into syngas.[81] Ni-based catalysts are considered cost-effective, efficient, and stable catalysts for dry reforming of CH_4.[82] Maybe due to this, many studies have

tried Ni loaded on mining waste support for dry reforming of CH_4. For instance, Chamoumi *et al.* conducted dry reforming of CH_4 using a Ni-loaded ilmenite metallurgical residue catalyst.[48] The ilmenite metallurgical residue primarily consisted of CaO, MgO, and MnO. The reaction was performed at 810 °C under atmospheric pressure for 4 h with a CH_4/CO_2 molar ratio of 1. The catalyst showed a CH_4 conversion of 87%, 84% CO yield, and 70% H_2 yield (entry 1, Table 4). The catalytic performance of the Ni/metallurgical residue catalyst was superior to that of a spinel ferrite ($NiFe_2O_4$). For a 7 d run, however, the catalyst lost its activity as the CH_4 conversion, CO yield and H_2 yield were decreased by 22%, 19%, and 25%, respectively. Calcination at 900 °C restored the catalytic properties, confirming the regenerability of the Ni-loaded ilmenite metallurgical residue catalyst.

Malik *et al.* prepared a Ni catalyst supported on metallurgical residue in both powder and pellet forms and compared their catalytic performance for dry reforming of CH_4.[70] The powder catalyst demonstrated superior performance under atmospheric pressure due to its higher surface area compared to the pelletized catalyst. However, under elevated pressures (at least 5.5 atm), the pelletized catalyst exhibited greater activity for syngas production (entries 2 and 3, Table 4). For instance, the pelletized catalyst achieved higher conversions of CH_4 and CO_2 and higher syngas yields than the powder catalyst within the pressure range of 5.5–6.5 atm. The improved catalytic performance of the pelletized catalyst under elevated pressures was attributed to increased coke oxidation rates, which mitigated coke deposition on the active sites. Nevertheless, a further increase in pressure from 6.5 to 10 atm resulted in reduced activity and selectivity of the pelletized catalyst, likely due to the formation of crystalline graphitic carbon, which caused the disintegration of the pellet particles.

Azara *et al.* prepared iron-rich mining residue-supported Ni catalysts with varying Ni loading for dry reforming of ethylene

Table 4 Performance of mining waste-supported Ni catalysts for syngas and H_2 production

Entry	Catalyst	Reaction	Reaction conditions	Performance	Ref.
1	Ni/metallurgical residue	Dry reforming of CH_4	T = 810 °C; P = 1 atm; t = 4 h; Q = 15 mL min^{-1}; SV = 2900 mL g^{-1} h^{-1}; CH_4/CO_2 = 1	CH_4 conversion = 87%; CO yield = 84%; H_2 yield = 70%	48
2	Ni/metallurgical residue (powder)	Dry reforming of CH_4	T = 800 °C; P = 5.5 atm; t = 4 h; GHSV = 810 L kg^{-1} h^{-1}; CH_4/CO_2 = 0.5	CH_4 conversion = 82%; CO_2 conversion = 53%; CO yield = 47%; H_2 yield = 54%	70
3	Ni/metallurgical residue (pellet)	Dry reforming of CH_4	T = 800 °C; P = 5.5 atm; t = 4 h; GHSV = 810 L kg^{-1} h^{-1}; CH_4/CO_2 = 0.5	CH_4 conversion = 85%; CO_2 conversion = 67%; CO yield = 62%; H_2 yield = 64%	70
4	Ni/iron-rich mining residue	Dry reforming of C_2H_4	T = 650 °C; P = 1 atm; t = 2 h; Q = 40 mL min^{-1}; GHSV = 4800 mL g^{-1} h^{-1}; C_2H_4/CO_2 = 3	C_2H_4 conversion = 91.29%; CO_2 conversion = 88.48%; H_2 yield = 67.47%	34
5	Ni/slag residue	Steam reforming of CH_4	T = 900 °C; P = 1 atm; t = 168 h; Q = 15 mL min^{-1}; SV = 3000 mL g^{-1} h^{-1}; H_2O/CH_4 = 1.7	CH_4 conversion = 98%; CO yield = 91%; H_2 yield = 92%	43
6	Ni/mining residue	Steam reforming of toluene	T = 800 °C; P = 1 atm; t = 24 h; WHSV = 4 h^{-1}; C/H_2O = 1	Toluene conversion = 98.3 wt%; CO yield = 74%; H_2 yield = 82%	71
7	Ni/iron-rich mining residue	Thermal decomposition of C_2H_4	T = 750 °C; P = 1 atm; t = 2 h; Q = 40 mL min^{-1}; GHSV = 4800 mL g^{-1} h^{-1}; C_2H_4/Ar = 3	Ethylene conversion = 92.24%; H_2 yield = 74.46%; carbon yield = 76.25%	34
8	Ni/slag residue	Sequential non-catalytic pyrolysis–catalytic decomposition of (1) virgin HDPE, (2) used HDPE, and (3) plastic mixture	T = 700 °C (1st stage) & 650 °C (2nd stage); t = 2 h; Q (N_2) = 0.03 SLPM; plastic feed rate = 0.33 g min^{-1}	(1) Gas yield = 33.13%; H_2 yield = 75.62% (2) Gas yield = 34.35%; H_2 yield = 79.40% (3) Gas yield = 36.08%; H_2 yield = 70.40%	42
9	Ni/coal gangue	Pyrolysis of polyethylene	(1) 1st stage (non-catalytic): T = 500 °C (10 °C min^{-1}); t = 20 min (2) 2nd stage (catalyst bed): T = 750 °C; Q = 100 mL min^{-1} N_2	H_2 yield = 31.48 mmol g^{-1}; H_2 concentration = 66.48 vol%	56
10	Iron ore tailings	Thermal cracking of oleic acid	T = 450 °C; P = 1.25 MPa Ar; t = 3 h; oleic acid/catalyst = 1 (w/w)	Gas yield = 95 mol%; H_2 selectivity = 68 mol%	80
11	Ni/metallurgical residue	Steam reforming of glycerol	T = 580 °C; P = 1 atm; GHSV = 10 966 cm^3 (STP) g^{-1} h^{-1}; water/glycerol = 9	Glycerol conversion = >99%; H_2 yield = 80.7%	73
12	Rh/metallurgical residue	Steam reforming of glycerol	T = 580 °C; P = 1 atm; GHSV = 10 966 cm^3 (STP) g^{-1} h^{-1}; water/glycerol = 9	Glycerol conversion = >99%; H_2 yield = 78%	74
13	Ru/metallurgical residue	Steam reforming of glycerol	T = 580 °C; P = 1 atm; GHSV = 10 966 cm^3 (STP) g^{-1} h^{-1}; water/glycerol = 9	Glycerol conversion = 94%; H_2 yield = 71%	74

T = temperature; P = pressure; t = time; Q = volumetric flow rate; SV = space velocity; GHSV = gas hourly space velocity.

(C_2H_4 + $2CO_2$ → $4CO$ + $2H_2$, ΔH°_{298} = 292.5 kJ mol^{-1}).[34] Higher Ni loading improved the activity of the catalyst for H_2 production. Specifically, the 13% Ni/iron-rich mining residue catalyst achieved a C_2H_4 conversion of 91.3%, a CO_2 conversion of 88.5%, and an H_2 yield of 67.5% under the following conditions: 650 °C, atmospheric pressure, a C_2H_4/CO_2 molar ratio of 3, and a gas hourly space velocity (GHSV) of 4800 mL g^{-1} h^{-1} for 2 h time-on-stream (entry 4, Table 4).

3.2.2. Steam reforming. Steam reforming produces syngas by reacting hydrocarbons (*e.g.*, CH_4 and toluene) with steam. Chamoumi and Abatzoglou utilized slag residue from metal mining (composed primarily of Fe, Mg, and Al) as a catalyst support to prepare a Ni catalyst for steam methane reforming (CH_4 + H_2O → CO + $3H_2$, ΔH°_{298} = 206 kJ mol^{-1};[83] entry 5, Table 4).[43] The reaction was conducted at 900 °C with a CH_4/H_2O molar ratio of 0.59 and a space velocity of 3000 mL g^{-1} h^{-1}. The catalyst achieved 98% CH_4 conversion, remaining stable over 168 h time-on-stream, with 92% H_2 yield and 91% CO yield (H_2/CO ratio of approximately 3). The high catalytic activity under the reducing environment of the reforming reaction was attributed to two key factors: (1) the formation of Fe–Ni alloys such as FeNi, FeNi$_3$, and Fe$_3$Ni$_2$, derived from the

reduction of NiFe$_2O_4$ and FeNiAlO$_4$, and (2) the solid solution of NiO–MgO, which provided an active Ni phase while preventing carbon deposition due to its alkalinity.

Belbessai *et al.* prepared a Ni catalyst supported on mining residue (entry 6, Table 4).[71] It was observed that in this catalyst, metallic Ni was protected by MgO present in the NiO/MgO solid solution due to strong metal–support interactions. The metallic Ni particles were on the nanometer scale and highly uniformly dispersed, effectively suppressing coke formation.[84] The catalyst's basicity, attributed to the presence of MgO, enhanced steam adsorption on the catalyst surface.[85] Other promoters present in the mining residue, such as Ca, further contributed to the improved catalytic activity. The catalyst was tested for the steam reforming of toluene as a model reaction for tar upgrading. Under reaction conditions of 800 °C and 1-day time-on-stream, the toluene conversion reached 98.3% with an H_2 yield of 82% and a CO yield of 74%.

3.3. H_2 production

Hydrogen (H_2) possesses a higher gravimetric energy density than conventional fuels such as natural gas, oil, and petrol.[86] It is considered a promising alternative energy resource,

serving as a clean and efficient energy carrier.[87] Table 4 (entries 7–13) summarizes studies on H_2 production from various feedstocks on mining waste-derived catalysts *via* thermal decomposition and glycerol reforming.

3.3.1. Thermal decomposition. Azara *et al.* synthesized a Ni catalyst (13% Ni loading) supported on iron-rich mining residue (entry 7, Table 4).[34] The catalyst was applied in the thermal decomposition of ethylene ($C_2H_4 \rightarrow 2C + 2H_2$, $\Delta H^{\circ}_{298} = 52.5 \text{ kJ mol}^{-1}$). The reaction was conducted for 2 h under 1 atm with a C_2H_4/argon ratio of 3 at 750 °C and a GHSV of 4800 mL g^{-1} h^{-1}. The catalyst yielded 74.5% H_2 at C_2H_4 conversion of 92.2%. In addition to H_2, thermal C_2H_4 cracking led to the formation of carbon deposited on the catalyst in 76.3% yield. Deposited carbon had a filamentous structure, which did not block the reactant's access to the catalyst's active sites. The iron species present on the mining residue support facilitated the growth of filamentous carbon, while Ni particles were responsible for cleaving C–C bonds in C_2H_4.

A catalyst prepared by loading Ni onto a metal mining slag residue was utilized in a sequential process combining non-catalytic pyrolysis and catalytic decomposition of plastics to produce H_2 as a plastic waste valorization strategy.[42] In this system, the plastic feedstock was thermally decomposed at 700 °C in the first stage, evolving a range of hydrocarbon products. These hydrocarbon products were then passed through the catalyst bed at 650 °C in the second stage, where they were converted into lighter compounds. In the second-stage reactor, the cleavage of C–H and C–C bonds primarily occurred at Ni and Ni–Fe alloy active sites. Various plastic feedstocks were tested, including virgin high-density polyethylene (HDPE), used HDPE, and a plastic mixture comprising 80 wt% PE, 15 wt% polypropylene, 4 wt% polystyrene and polyethylene terephthalate (PET), and 1 wt% miscellaneous. Over the catalyst, the HDPE feedstocks achieved H_2 yields of 75–79% with gas yields of 33–34 wt%, while the plastic mixture produced a H_2 yield of 70.4% with a gas yield of 36 wt% under comparable reaction conditions (entry 8, Table 4).

Zhang *et al.* prepared Ni catalysts supported on coal gangue used for pyrolysis of polyethylene (PE) (entry 9, Table 4).[56] Pyrolysis was carried out using a two-stage fixed bed reactor involving the 1st reactor that pyrolyzed PE at 500 °C and the 2nd reactor that catalytically decomposed pyrolytic volatiles evolved from PE. Different catalyst temperatures (700–900 °C) and Ni loadings (5–20%) were tested, showing that the 15% Ni/coal gangue catalyst led to the highest H_2 yield of 31.5 mmol g^{-1} with 66.5 vol% concentration at 750 °C. The catalyst could be regenerated through oxidation, and it was reusable for at least five cycles, retaining a H_2 yield of 27 mmol g^{-1} with 63 vol% concentration.

Luciano *et al.* used iron ore tailings rich in iron oxides and SiO_2 for catalytic thermal decomposition of fatty acid (*e.g.*, oleic acid) under a high pressure (entry 10, Table 4).[80] The iron ore tailings were directly used as the catalyst with no treatment. In the presence of the catalyst, oleic acid was converted mainly into a gaseous product composed mainly of H_2 at 450 °C under 1.25 MPa Ar for 3 h with an oleic acid/catalyst

weight ratio of 1, achieving 95 mol% gaseous product yield and 68 mol% H_2 selectivity.

3.3.2. Glycerol reforming. Studies conducted by Iliuta and co-workers investigated the steam reforming of glycerol ($C_3H_8O_3 + 3H_2O \rightarrow 3CO_2 + 7H_2$, $\Delta H^{\circ} = 123 \text{ kJ mol}^{-1}$) over Ni catalysts supported on metallurgical waste consisting of Al, Fe, and Mg, crystallized in mixed oxide spinel groups such as $FeAl_2O_4$ and $MgFe_2O_4$.[72,73] 5 wt% Ni supported on the metallurgical waste resulted in nearly complete conversion of glycerol into gaseous products at 580 °C with a H_2 yield of 80.7% (entry 11, Table 4). Coke formation was minimized at this temperature, with a measured coke deposition rate of 0.59 mg_{coke} h^{-1} m^{-2} g^{-1}. Increasing the reaction temperature to 730 °C further suppressed coke formation (to 0.18 mg_{coke} h^{-1} m^{-2} g^{-1}) by limiting the Boudouard reaction, but the H_2 yield decreased to 59.4%.[73] The high catalytic activity for H_2 production and coke suppression was attributed to the synergistic interaction between Ni and Fe/Mg species in the metallurgical waste support, leading to the formation of active Ni–Fe_xO_y and Ni–MgO sites. Additionally, the activation energy for glycerol steam reforming on the Ni catalyst was calculated to be 66.1 kJ mol^{-1}, with a partial reaction order regarding glycerol of 0.63.[88]

The Ni catalyst was compared with Rh and Ru catalysts for H_2 production from glycerol *via* steam reforming.[74] The Ni catalyst demonstrated superior performance for hydrogen production compared to the Rh and Ru catalysts (entries 11–13, Table 4). Fig. 2 illustrates the cooperative interactions between the incorporated metal (Ni, Rh, or Ru) and the Fe/Mg-bearing species present on the mining waste support surface, which play a critical role in glycerol activation and promote its reforming. The regenerative mechanism (Fig. 2b) is CO conversion into CO_2 by reacting with the oxygen produced by water dissociation or with the support's lattice oxygen.[89] However, the presence of alkaline or alkaline-earth metals on the catalyst surface can promote an associative mechanism (Fig. 2a),[90] which facilitates the conversion of CO and water. For Rh-based catalysts, the reaction pathway is believed to involve the formation of COO–formate species on Fe_xO_y species in close proximity to metallic Rh,[91] promoting CO_2 and H_2 production. Similarly, an associative mechanism is also supported for reactions occurring on MgO.[92] The results showed that the degree of interaction between the incorporated metal and MgO on the catalyst surface was strongly correlated with hydrogen production. The Ru catalyst exhibited the lowest H_2 yield, which was attributed to its poor propensity for MgO–RuO_2 interactions on the catalyst surface.

4. Chemical conversion using mining waste-derived catalysts

4.1. Mining waste catalysts prepared for various chemical conversion reactions

Section 3 introduced that various mining waste could be used as a catalyst support for preparing supported Ni catalysts
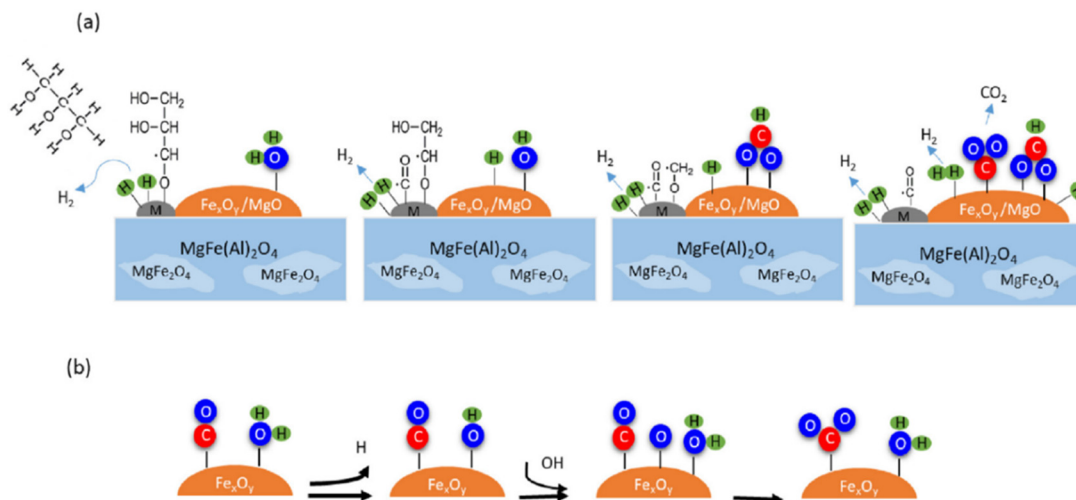
Fig. 2 Proposed mechanism of glycerol reforming over metallurgical waste-supported metal (M) catalysts through (a) associative and (b) regenerative mechanisms. Reprinted from Sahraei et al.,[74] copyright (2021), with permission from Elsevier.

employed for the production of syngas and H_2. In this section, various mining waste catalysts or mining waste-supported metal catalysts are discussed for different chemical conversion reactions such as esterification, hydrodeoxygenation (HDO), nitrogen oxides (NO_x) removal, carbon monoxide (CO) oxidation, and carbon dioxide (CO_2) reduction, as summarized in Table 5.

For certain reactions (e.g., CO oxidation and CO_2 reduction), supported metal catalysts (e.g., Cu, Ni, and Au) were prepared by an impregnation or precipitation method (entries 1–3, Table 5). Several mining wastes could be employed as catalysts

themselves after pre-treatment (entries 4–8, Table 5). Pre-treatment involved acid and/or base treatment in order to activate catalytic sites and remove impurities. For example, iron mining waste (major mineral phase of hematite and quartz) treated with H_2SO_4 or ammonium sulfate ((NH_4)$_2SO_4$) resulted in catalysts with varying surface acid densities—the H_2SO_4-treated catalyst exhibited a surface acid density approximately 4 times higher than the (NH_4)$_2SO_4$-treated one.[35] This difference is attributed to the enhanced solubilization of iron species in sulfuric acid, leading to the formation of highly dispersed iron sulfate groups upon calcination (Fig. 3). Treatment

Table 5 Mining waste catalysts used for various chemical conversion reactions

Entry	Mining waste (major components)	Treatment	Surface area ($m^2 g^{-1}$)	Total pore volume ($cm^3 g^{-1}$)	Average pore diameter (nm)	Surface acid site ($mmol\ g^{-1}$)	Ref.
1	Rare Earth tailings (Fe_2O_3, CaO, SiO_2, MgO)	Ni and Cu loadings = 2% and 2.5%, respectively	63.78	0.12	7.82	3.96	53
2	Tailings and slags (FeO)	Au loading (1 wt%)	63.8	0.076	1.6	—	41
3	Coal gangue (SiO_2, Al_2O_3, Fe_2O_3)	Ni loading (15 wt%)	9.1	0.0126	56.03	—	57
4	Iron mining tailings (Fe oxides)	H_2SO_4 treatment	—	—	—	0.1211	35
5	Kaolin waste (SiO_2, Al_2O_3)	H_2SO_4 treatment; hydrothermal treatment at 110 °C in the presence of NaOH & CTAB; functionalization with MPS	998–1016	0.78–0.80	3.14–3.25	5.93	54, 55 and 93
6	Bauxite mining waste (Fe oxides, Al_2O_3, SiO_2, TiO_2)	A form of non-alkaline magnetic solid	—	—	—	—	45
7	Rare Earth tailings (Fe_2O_3, CaO, SiO_2, MgO)	Na_2CO_3/Ca(OH)$_2$ treatment	—	—	—	—	51
8	Mixture of rare Earth tailings and concentrate (1/1, w/w; Fe_2O_3, CaO, SiO_2, MgO)	Na_2CO_3/Ca(OH)$_2$ treatment, followed by HCl/citric acid treatment	7.69	0.0403	17.44	—	52

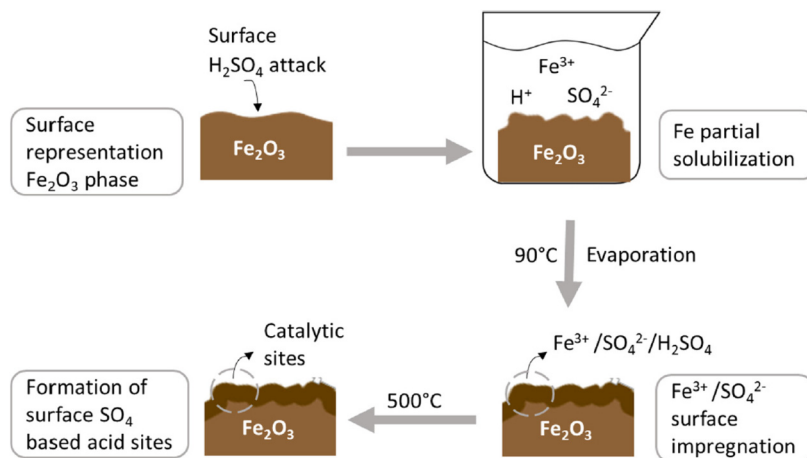CTAB = cetrimonium bromide. MPS = 3-mercaptopropyltrimethoxysilane.

Fig. 3 Schematic description of catalyst preparation from iron ore tailings for the esterification reaction. Reprinted from Prates *et al.*,[35] copyright (2020), with permission from Elsevier.

with Na_2CO_3 and $Ca(OH)_2$ increased the Fe_2O_3 content in rare Earth tailings that acted as active sites for denitrification.[51] The addition of HCl and citric acid to the Na_2CO_3/$Ca(OH)_2$-treated catalyst modified the surface morphology of the mineral, increased the number of active sites, and enhanced the adsorption of NH_3, which was beneficial for the selective catalytic reduction of NO_x using NH_3 as a reducing agent (NH_3-SCR).[52]

Beyond simple pretreatment with acid and base, Nascimento's group used kaolin waste to synthesize high-surface-area functionalized mesoporous aluminosilicates used for esterification reactions.[54,55,93] The synthesis procedure involved acid leaching, hydrothermal treatment in the presence of NaOH and cetrimonium bromide, and then functionalization with 3-mercaptopropyltrimethoxysilane. The material exhibited a higher surface area of >900 m² g⁻¹ with the organic functional group ($-SO_3H$) leading to a high density of surface acid sites, which gave high esterification activities for different feedstocks.

4.2. Esterification

Esterification of free fatty acids (FFAs) with alcohol using an acid catalyst is a key reaction in the production of biodiesel, a renewable alternative to petroleum-derived diesel fuels.[94] A variety of solid acid catalysts have been used for esterification of FFAs, including acidic organic resins, zeolites, mesoporous silicate, heteropolyacids, sulfated metal oxides, and binary metal oxides.[95] Some of the components contained in these solid acids (*e.g.*, metal oxides) are also contained in mining waste (Table 2); thus, mining wastes with proper treatment/functionalization have been applied to esterifying FFAs (entries 1–4, Table 6). For instance, Prates *et al.* investigated the use of iron ore tailings-derived catalysts for the esterification of oleic acid as a surrogate reaction for biodiesel production using mining waste-derived catalysts.[35] At 120 °C for 4 h of reaction, the H_2SO_4-impregnated catalyst achieved complete conversion (100%) of oleic acid into its corresponding

ester under a methanol/oleic acid molar ratio of 15 and 5 wt% catalyst loading (entry 1, Table 6).

A by-product of kaolin extraction mining was utilized to synthesize a high-surface-area mesoporous aluminosilicate functionalized with $-SO_3H$ groups for catalytic applications, including esterification of palm oil distillate and acetylation of eugenol.[93] The palm oil-derived feedstock contained 84% FFAs. During the esterification process, increasing the reaction temperature from 110 to 130 °C and extending the reaction time from 30 min to 2 h significantly improved the conversion of FFAs. The catalyst achieved up to 95% conversion of FFAs into fatty acid ethyl esters at 130 °C for 2 h under a molar ratio of ethanol to palm oil distillate of 30 and 4% catalyst loading (entry 2, Table 6). Additionally, the catalyst demonstrated re-usability for at least four cycles, maintaining a conversion efficiency greater than 73%. The same catalyst was also applied to the acetylation of eugenol using acetic anhydride as the acetylating agent.[55] The catalyst could convert 99.9% of eugenol into eugenyl acetate under optimized conditions (80 °C, 40 min, acetic anhydride/eugenol molar ratio of 5, and 2% catalyst loading; entry 3, Table 6). Successive reuse of the SO_3H-functionalized aluminosilicate catalyst for the acetylation of eugenol resulted in a gradual decline in eugenol conversion, decreasing to 90% after 4 cycles. This reduction in efficiency is most likely due to active sites being occupied by molecules from reactants or products. A SO_3H-functionalized aluminosilicate catalyst synthesized from kaolin waste was also employed for the esterification of industrial waste from palm oil deodorization (entry 4, Table 6).[54] The esterification reaction was conducted at 130 °C for 2 h with a methanol/fatty acid molar ratio of 30 and 5% catalyst loading, achieving 98% conversion of palm oil deodorization waste into esters. In contrast, the non-catalytic reaction under identical conditions converted only 15% of the feedstock, highlighting the catalyst's effectiveness. After use, the catalyst was recovered and reused in the same reaction, yielding 81% conversion of the palm oil waste. This decline in performance indicates the need for

Table 6 Performance of mining waste catalysts for various chemical conversion reactions

Entry	Catalyst	Reaction	Reaction conditions	Performance	Ref.
1	H_2SO_4-impregnated iron tailings	Esterification of oleic acid	T = 120 °C; t = 4 h; catalyst loading = 5 wt%; methanol/oleic acid molar ratio = 15	Oleic acid conversion = 100%	35
2	SO_3H-functionalized flint kaolin	Esterification of palm oil distillate	T = 130 °C; t = 2 h; catalyst loading = 4%; ethanol/palm oil distillate molar ratio = 30	Palm oil distillate conversion = 95%	93
3	SO_3H-functionalized flint kaolin	Acetylation of eugenol	T = 80 °C; t = 40 min; catalyst loading = 2%; eugenol/acetic anhydride molar ratio = 0.2	Eugenol conversion = 99.9%	55
4	SO_3H-functionalized kaolin waste	Esterification of palm oil deodorization waste	T = 130 °C; t = 2 h; catalyst loading = 5%; methanol/fatty acid molar ratio = 30	Palm oil deodorization waste conversion = 98%	54
5	Reduced bauxite mining waste	Hydrodeoxygenation of levulinic acid	T = 365 °C; t = 4 h; 50 wt% aqueous solution; initial H_2 pressure = 5.5 MPa catalyst loading = 9.1 wt%	C_9 alkane and alkene yield = up to 76 wt%	45
6	Alkali/acid co-treated rare Earth tailings	Denitrification	T = 900 °C; $C_{NO,i}$ = 500 ppm; Q = 500 mL min^{-1}; CO/NO ratio = 4	NO removal efficiency = 96.2%	51
7	Alkali/acid co-treated rare Earth tailings	NH_3-SCR	T = 350 °C; Q = 100 mL min^{-1} (3% O_2, SV = 25 000 h^{-1}); NH_3/NO ratio = 1	NO removal efficiency = 82%	52
8	Ni–Cu/rare Earth tailings	NH_3-SCR	T = 300 °C; Q = 100 mL min^{-1} (3% O_2, SV = 8000 h^{-1}); NH_3/NO ratio = 1	NO removal efficiency = 90%; N_2 selectivity = 85%	53
9	Au/yellow hematite	CO oxidation	T = 62 °C; Q = 50 mL min^{-1}; W/F = 0.36 g s mL^{-1}; CO/O_2 = 1/20	CO conversion = 90%	41
10	Ni/coal gangue	CO_2 methanation	T = 450 °C; Q = 100 mL min^{-1}; WHSV = 30 000 mL g^{-1} h^{-1}; CO_2/H_2 = 1/4	CO_2 conversion = 73%; CH_4 selectivity = 91%	57

T = temperature; t = time; Q = volumetric gas flow rate; SV = space velocity; W/F = weight of catalyst/the total flow rate of the reactant gas.

further research to optimize the mining waste-derived catalyst, particularly in terms of improving its stability during successive reaction cycles.

4.3. Hydrodeoxygenation

HDO is a representative important reaction in biomass conversion and bio-oil upgrading, which reduces the oxygen content of biomass-derived products.[96] Typically, bi-functional catalysts consisting of metal and solid acid sites have been employed for HDO of biomass feedstocks.[97] One study could be found that was conducted by using a mining waste-derived catalyst for HDO.[45] Bauxite mining waste, comprising a highly alkaline mixture of Fe_2O_3 (>60 wt%), TiO_2, and complicated sodium alumino-silicates was employed as a catalyst that underwent *in situ* reduction at 350 °C. The reduced bauxite mining waste was found to be a non-alkaline magnetic solid. The catalyst was then used for HDO of levulinic acid (a well-known chemical derived from biomass) into a blend of C_9 alkanes and alkenes with up to 76 wt% yield at 365 °C and an initial pressure of 5.5 MPa H_2 (entry 5, Table 6). It could be re-used without loss of activity at least five times.

4.4. NO$_x$ removal

NO$_x$ (*e.g.*, NO and NO_2) are a major component of kerbside pollution in large cities and in roadway microenvironments.[98] Also, reprocessing spent nuclear fuel produces high-level radioactive liquid waste containing HNO_3, which needs to be reduced to gas products by adding formaldehyde, resulting in the formation of NO$_x$ emitted *via* exhaust gas.[99] In such applications, NO$_x$ removal is crucial. A variety of supported metal catalysts (*e.g.*, Pt, Mn, Mo, V, Fe, Cu, and Ce) and binary metal oxides (*e.g.*, CeO_2/TiO_2, MnO_x/CeO_2–ZrO_2–Al_2O_3, and SnO_2–

MnO_x–CeO_2) have been used as NO$_x$ removal catalysts.[100] There have been a few studies on using mining waste-derived catalysts for NO$_x$ removal.

Wang *et al.* reported the denitrification performance of a catalyst derived from rare Earth tailings.[51] To prepare the catalyst, rare Earth tailings underwent co-treatment with an alkali (calcium hydroxide and sodium carbonate) and an acid (HCl and citric acid) followed by calcination at 500 °C. The co-treatment process increased the Fe_2O_3 content in the catalyst, which played a crucial role in the denitrification reaction. Notably, the reduction temperature of the modified catalyst was higher than that of the original rare Earth tailings, indicating improved thermal stability. The catalyst achieved 96.2% efficiency for NO removal (initial NO concentration of 500 ppm, CO/NO = 4) at 900 °C (entry 6, Table 6). In the denitrification reaction over the catalyst, Fe_2O_3 is reduced to FeO by adsorbing CO molecules, while FeO is oxidized to Fe_2O_3 by adsorbing NO molecules (Fig. 4). Meanwhile, NO is reduced to N_2. This redox capacity could enable continuous operation of the denitrification reaction.

NH_3-SCR, considered one of the most efficient technologies for NO$_x$ removal from flue gas emitted by stationary and mobile sources,[101] has been conducted using mining waste-derived catalysts.[52,53] For example, a catalyst was synthesized from a mixture of rare Earth tailings and concentrate, containing cerium oxides and Fe–Ce composite oxides.[52] The acid and alkali treatments increased the contents of Fe^{2+}, Ce^{3+}, and lattice oxygen, which significantly influenced the catalyst's NO degradation performance. Under controlled reaction conditions (entry 7, Table 6), the catalyst achieved 82% NO removal efficiency. A bimetallic Ni–Cu/rare Earth tailings catalyst was also applied for NH_3-SCR (entry 8, Table 6).[53] The
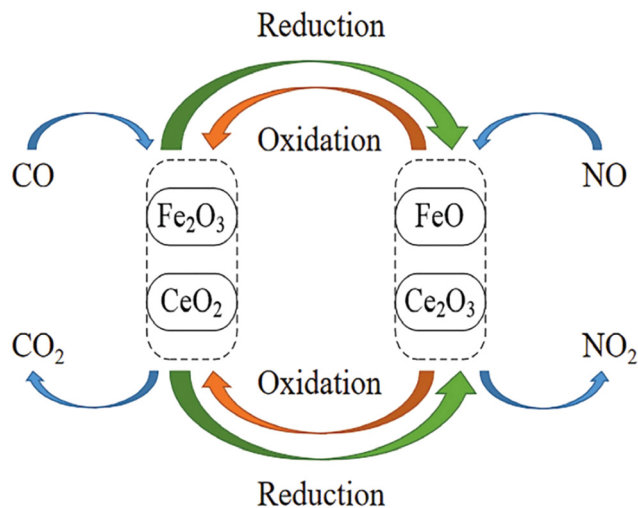
Fig. 4 Schematic description of the catalytic denitrification reaction. Reprinted from Wang *et al.*[51] and licensed under CC BY 4.0.

addition of Ni and Cu introduced strong electron interactions between Fe, Ni and Cu, resulting in electron transfer between Ni–Fe and Cu–Fe and the subsequent formation and adsorption of nitrate species. Moreover, the formation of the $NiFe_2O_4$ spinel structure increased the number of surface-active sites, while the bimetallic Ni–Cu sites enhanced oxygen vacancies in CuO, improving the redox ability of the catalyst. The optimal composition of the bimetallic catalyst was found to be 2% Ni–2.5% Cu/rare Earth tailings, achieving a NO removal efficiency of 90% at 300 °C.

4.5. CO oxidation

CO gas, emitted from diverse sources, such as vehicle exhaust and industrial activities, poses significant risks to both the environment and human health.[102] Thus, there have been continuous demands for the development of highly efficient and sustainable catalysts to mitigate CO emissions. CO oxidation is an attractive approach for eliminating CO from exhaust gas and in the fields of gas masks, gas sensors, and catalytic converters in fuel cells.[103,104] In this regard, efforts were made to utilize mining waste originating from ore mines as CO oxidation catalysts. In a recent study by Mpiliou *et al.*,[41] mesoporous iron oxide (*e.g.*, hematite) derived from Serifos Fe-skarns mining waste was used as a catalyst support loaded with Au nanoparticles. The mining waste was calcined at 300 °C to remove impurities such as goethite, resulting in a more stable hematite support with a high surface area of up to 98.8 m^2 g^{-1}. Au nanoparticles were well-dispersed on the mining waste-derived hematite through a deposition–precipitation method. This catalyst achieved 90% CO conversion during the CO oxidation reaction at approximately 62 °C (entry 9, Table 6).

4.6. CO₂ methanation

Reducing CO_2 emissions is an essential global challenge in the fight against climate change.[105,106] CO_2 methanation is con-

sidered a cost-effective method of CO_2 reduction *via* the Sabatier reaction ($CO_2 + 4H_2 \rightarrow CH_4 + 2H_2O$, $\Delta H° = -164$ kJ mol^{-1}).[107] The Sabatier reaction is thermodynamically favorable at ambient temperature, but the production of CH_4 is limited by the slow kinetics of this reaction. This necessitates the use of an active and selective catalyst.[107] For CO_2 methanation, Bahraminia and Anbia prepared Ni catalysts with different Ni loadings (5–20%) using coal gangue as the catalyst support.[57] The coal gangue-supported Ni catalysts were used for the conversion of CO_2 into CH_4 at 450 °C and atmospheric pressure with 30 000 mL g^{-1} h^{-1} of WHSV consisting of 60% H_2/15% CO_2/25% Ar (entry 10, Table 6). The mining waste-derived Ni catalyst with 15% Ni achieved 73% CO_2 conversion and 91% CH_4 selectivity. An increase in Ni loading from 5% to 15% increased the CO_2 conversion and CH_4 selectivity due to an increase in the number of active sites, but a further increase in Ni loading to 20% decreased the conversion and selectivity due to an increase in Ni particle size leading to blocking of the support cavities.

5. Wastewater treatment using mining waste-derived catalysts

5.1. Mining waste catalysts prepared for wastewater treatment

Mining waste-derived catalysts can also serve as effective materials for wastewater treatment.[108] Recently, research has focused on recycling waste resources and modifying them into catalysts to efficiently remove pollutants from water. The preparation of mining waste-based catalysts for wastewater treatment commonly involves processes such as impurity removal, grinding, homogenization, and calcination. In some studies, additional salts and chemicals are added during synthesis to enhance catalytic properties.[109] These catalysts have been successfully applied in Fenton, photo-Fenton, peroxymonosulfate (PMS) activation, electrochemical processes, and ozonation for pollutant removal from wastewater.

In the wastewater treatment process, mining waste is converted into catalysts through various catalytic synthesis methods, as shown in Table 7. In some studies, untreated mining waste was used directly as a catalyst through grinding and milling (entries 5–7 and 9, Table 7). Conversely, in entries 2 and 3, HNO_3 or $CHBr_3$ was added to modify the mining waste. The addition of these chemicals enhances the purity[110] of the modified catalyst by decomposing the mining waste through acid treatment or separating it *via* density separation.[111] Furthermore, in most studies, the catalyst was modified using hydrothermal or thermal treatment (entries 1, 4, 8 and 10–15, Table 7). Thermal treatment removes volatile impurities from the mining waste and increases the number of active sites by altering the crystal structure.[112] Catalysts modified through thermal treatment generally exhibited high specific surface areas, ranging from 20 to 63.48 m^2 g^{-1}. Various metal oxides and minerals, including Fe oxides (*e.g.*, Fe_2O_3 and Fe_3O_4), SiO_2, and Al_2O_3, were primarily present in

Table 7 Mining waste catalysts used for wastewater treatment

Entry	Mining waste (major components)	Treatment	Surface area ($m^2\ g^{-1}$)	Total pore volume ($cm^3\ g^{-1}$)	Average pore diameter (nm)	Crystallite size (nm)	Saturation magnetization (M_s; emu g^{-1})	Ref.
			Properties					
1	Bauxite mining tailings (Fe oxides)	Fe^{3+} and Fe^{2+} molar ratio = 2 : 1 Hydrothermal treatment at 150 °C Thermal treatment at 400 °C	—	—	—	γ-Fe_2O_3 = 71.3; Fe_3O_4 = 61.3	9.8	46
2	Pyritic waste (FeS_2, SiO_2, Al_2O_3, CaO, K_2O, Cr_2O_3)	$CHBr_3$ purification	2.37	0.0056	10 900	—	—	49
3	Pyrite waste (SO_3, Fe_2O_3, SiO_2, Al_2O_3, Na_2O_3)	HNO_3 treatment	11.614	6.339	1.57	—	—	113
4	Iron mining residue (SiO_2, FeO)	Thermal treatment at 600 °C under an atmosphere of CH_4	4.0	—	—	—	—	36
5	Amethyst mining reject (SiO_2, Fe_2O_3, Al_2O_3, CaO, TiO_2)	—	16.35	0.047	11.65	—	—	44
6	Ilmenite mining residue (Fe oxides, $FeTiO_3$, $FeSi_2$, $CaTiSiO_5$)	—	0.6	—	—	—	—	114
7	Iron mining residue (Fe_2O_3, Ce_2O_3)	—	26	—	—	—	—	115
8	Iron mining waste (Fe_2O_3, SiO_2, CaO, B_2O_3, Al_2O_3)	Thermal treatment at 500 °C in air	50.6	0.055	4.944	—	—	112
9	Basalt mine tailings (SiO_2, Fe_2O_3, CaO, Al_2O_3)	—	13.43	0.033	9.73	—	—	47
10	Waste ore (Fe_3O_4, Co_3O_4, SiO_2, MgO)	Thermal treatment at 600 °C under an atmosphere of N_2	11.26	—	Meso = 4.18; macro = 61.87	—	7.42	33
11	Iron mining waste (Fe oxides, g-C_3N_4, SiO_2)	Suspension with melamine in H_2O Thermal treatment at 550 °C	59.0	—	—	—	—	38
12	Coal gangue (Al_2O_3, SiO_2, Fe_2O_3, SO_3)	Suspension with melamine in H_2O Thermal treatment at 550 °C	23.63	—	2–5	—	—	58
13	Pumice mining waste (SiO_2, Al_2O_3, K_2O)	Surface coating of nano-pumice onto carbon cloth Thermal treatment at 160 °C	63.48	0.117	—	—	—	50
14	Magnetic mining waste (Fe_2O_3, TiO_2, SiO_2, P_2O_5, CaO)	Polymerization with metakaolin at a ratio of 2.78 in the presence of NaOH and H_2O	10.4	1.05	40.26	—	18	39
15	Magnetic mining waste (Fe_2O_3, TiO_2, SiO_2, P_2O_5, CaO)	Polymerization with metakaolin at a ratio of 0.96 in the presence of NaOH and H_2O	20.0	1.76	35.13	—	—	40

the water treatment catalyst synthesized from mining waste. This composition closely resembles the mining waste components summarized in Table 2. Due to the presence of these metal-based compounds, some catalysts exhibited magnetic properties (entries 1, 10 and 14, Table 7). This magnetism enables easy catalyst separation after wastewater treatment, thereby improving catalyst reuse.

The synthesized catalyst generated reactive oxygen species (OH•, $SO_4^{•-}$, $O_2^{•-}$, $^1O_2$, *etc.*) for pollutant decomposition in various water treatment processes. Additionally, the efficiency of reactive oxygen species generation and pollutant decomposition varied based on the catalyst characteristics, leading to

an analysis of the optimal conditions and decomposition mechanisms for effective pollutant removal.

5.2. Fenton process

In the Fenton process, iron compounds such as Fe_2O_3, Fe_3O_4, FeO, and FeS_2 included in catalysts play a pivotal role in determining the efficiency of pollutant degradation. These iron compounds react with hydrogen peroxide (H_2O_2), an oxidizing agent, leading to the oxidation of Fe^{2+} to Fe^{3+} and the subsequent formation of OH• radicals. Additionally, Fe^{3+} is reduced back to Fe^{2+} as it interacts with either the oxidizing agent or the pollutants, further enhancing radical gene-

ration.[116] The OH• radicals produced through these reactions rapidly interact with pollutants, significantly improving the decomposition performance of the Fenton process.

Santosa *et al.* synthesized magnetic catalysts *via* applying the hydrothermal method to the immobilized iron oxide precursor of Fe^{2+} and Fe^{3+} under alkaline conditions, followed by calcination.[46] When the concentration of H_2O_2 was 1 mM and the pH was 7, these conditions proved to be optimal for tetracycline removal, achieving a decomposition rate of 89.7% (entry 1, Table 8). Additionally, the catalyst could be easily separated using its magnetic properties, and its practicality was further demonstrated by minimal crystal structure deformation after use. On the other hand, Cechinel *et al.* utilized bromoform for density separation to eliminate impurities from pyrite, which was subsequently used as a catalyst for organic dye discoloration.[49] The use of bromoform effectively reduced impurities and enhanced the exposure of active sites by increasing access to the organic content in pyrite. As a result, the catalyst achieved a removal rate of 98% for reactive blue 21 dye under optimized conditions, with an H_2O_2 concen-

tration of 2 g L^{-1} at pH 4.7 (entry 2, Table 8). Also, this high pollutant removal efficiency was attributed to the enhanced conductivity and electron transfer properties imparted by Si and S oxides, which contributed to increased radical generation *via* Fe oxide reactions.[117] Mashayekh-Salehi *et al.* synthesized a catalyst from pyrite waste[113] and improved its performance by eliminating surface impurities through HNO_3 treatment, followed by milling. With a high FeS_2 purity, the catalyst exhibited maximum tetracycline removal and catalytic efficiency of 96.1% under optimal conditions, specifically at a solution pH of 4.1 and an H_2O_2 concentration of 5 mM (entry 3, Table 8). Tetracycline removal reached approximately 96.1%, and after four consecutive reuse cycles of pyrite, the removal efficiency remained above 90%. This stability was due to high catalytic activity and low iron leaching, which ensured sustained performance even after multiple cycles. In the study by Augusto *et al.*, iron mining residue was modified through calcination at 600 °C for 30 min under an atmosphere of methane. The catalyst indicated high thermal stability, presenting a negligible weight loss (<1%) in thermogravimetric analysis. The

Table 8 Performance of mining waste-derived catalysts for wastewater treatment

Entry	Catalyst	Reaction	Reaction conditions	Performance	Ref.
1	γ-Fe_2O_3/Fe_3O_4-bauxite mining tailings	Fenton	T = 25 °C; t = 120 min; C_{TC} = 20 mg L^{-1}; CD = 1.2 g L^{-1}; $C_{H_2O_2}$ = 1.0 mM; pH = 7	Tetracycline removal = 89.7%	46
2	Pyritic waste	Fenton	T = 20 °C; t = 210 min; C_{RB21} = 150 mg L^{-1}; CD = 0.5 g L^{-1}; $C_{H_2O_2}$ = 2 g L^{-1}; pH = 4.7	Reactive blue 21 removal = 98%	49
3	Pyrite waste	Fenton	T = 40 °C; t = 60 min; C_{TC} = 50 mg L^{-1}; CD = 1 g L^{-1}; $C_{H_2O_2}$ = 5 mM; pH = 4.1	Tetracycline removal = 96.1%	113
4	CH_4–iron mining residue	Fenton	t = 150 min; $C_{pollutants}$ = 10 mg L^{-1}; CD = 1 g L^{-1}; $C_{H_2O_2}$ = 6.2 M; pH = 7.2	Rhodamine b removal = >90%; paracetamol removal = >90%	36
5	Iron-bearing mining reject	Photo-Fenton	T = 25 °C; t = 180 min; C_{phenol} = 50 mg L^{-1}; CD = 0.75 g L^{-1}; $C_{H_2O_2}$ = 7.5 mM; pH = 3; light flux = 52.5 W m^{-2} (400–1000 nm)	Phenol removal = 96.5%	44
6	Ilmenite mining residue	Photo-Fenton	T = 25 °C; t = 30 min; $C_{pollutants}$ = 200 µg L^{-1}; CD = 0.277 mg L^{-1}; $C_{H_2O_2}$ = 65.4 mg L^{-1}; pH = 3.4; light flux = 6.8 W m^{-2} (350–400 nm)	Sulfamethoxazole removal = 89%; ciprofloxacin removal = 83%; tetracycline removal = 88%	114
7	Iron mining residue	Photo-Fenton	t = 60 min; C_{STZ} = 100 µg L^{-1}; CD = 0.3 g L^{-1}; $C_{H_2O_2}$ = 1 mM; pH = 2.5; light flux = 18 W m^{-2} (320–400 nm)	Sulfathiazole removal = 96%	115
8	Iron mining waste	Photo-Fenton	T = 25 °C; t = 90 min; $C_{SG\ dye}$ = 10 mg L^{-1}; CD = 0.15 g L^{-1}; $C_{Na_2SO_3}$ = 0.45 mM; pH = 3	Sicomet green dye removal = 91.5%	112
9	Basalt mine tailings	Photo-Fenton	T = 25 °C; t = 60 min; C_{P4R} = 50 mg L^{-1}; CD = 0.75 g L^{-1}; $C_{H_2O_2}$ = 4.5 mM; pH = 3	Ponceau 4R removal = 97.0%	47
10	Biochar-waste ore	PMS activation	t = 60 min; C_{TC} = 20 mg L^{-1}; CD = 0.9 g L^{-1}; C_{PMS} = 0.6 g L^{-1}; pH = 5	Tetracycline removal = 96.6%	33
11	Graphitic carbon nitride–iron mining waste	PMS activation	T = 25 °C; t = 60 min; C_{APAP} = 10 mg L^{-1}; CD = 0.5 g L^{-1}; C_{PMS} = 0.6 mM; pH = 6.5	Acetaminophen removal = 98%	38
12	Graphitic carbon nitride –coal gangue	PMS activation	T = 25 °C; t = 30 min; C_{BPA} = 50 mg L^{-1}; CD = 1.0 g L^{-1}; C_{PMS} = 0.27 mM; pH = 7	Bisphenol A removal = 90%	58
13	Microbial fuel cells–pumice mine waste	Electrochemical	T = 35 °C; t = 3 d; C_{COD} = 12 000 mg L^{-1}, BOD/COD = 0.4; electrode = 2 × 2 cm; catholyte = 50 mM (phosphate buffer); pH = 7	Generated voltages = 1.126 V; COD removal = 94%	50
14	Geopolymer–magnetic mining waste	Ozonation	T = 25 °C; t = 30 min; CD = 0.1 g L^{-1}; pH = 4	Ozone decomposition rate = 2.98 min^{-1}	39
15	Geopolymer–magnetic mining waste	Ozonation	T = 25 °C; t = 60 min; C_{TMP} = 1 g L^{-1}; CD = 0.1 g L^{-1}; pH = 4	Trimethoprim removal = 71%	40

T = temperature; t = time; CD = catalyst dosage; C_A = concentration of A.

iron mining residue is primarily composed of SiO_2, Fe_2O_3, and FeOOH, while calcination with CH_4 transforms the catalyst into a reduced iron phase of FeO.[118] The formation of Fe^{2+} enhances the removal efficiency to over 90%, as Fe^{2+} directly reacts with H_2O_2 at pH 7.2 and with 6.2 M of H_2O_2 (entry 4, Table 8).[36] The higher efficiency compared to the raw catalyst is due to the faster H_2O_2 decomposition rate with Fe^{2+} and a higher radical generation rate. As illustrated in Fig. 5, the use of the catalyst in combination with H_2O_2 consistently resulted in higher removal efficiency compared to the use of H_2O_2 alone, while the extent of variation depends on the pH.

5.3. Photo-Fenton process

The photo-Fenton process closely resembles the conventional Fenton process, where iron oxides serve as activators for the oxidant reagent. In this process, Fe^{2+} reacts with H_2O_2 to generate OH• radicals while being oxidized to Fe^{3+}. Among the iron oxides, Fe_2O_3 was identified as the primary component driving the reaction, highlighting its significance in the photo-Fenton mechanism. Unlike the standard Fenton process, where Fe^{3+} must be reduced back to Fe^{2+} through additional reagents, the photo-Fenton process utilizes light irradiation to rapidly reduce Fe^{3+} to Fe^{2+}, ensuring a continuous cycle of radical generation.[119] This self-sustaining reaction eliminates the need for an additional catalytic regeneration step, reducing catalyst consumption while maintaining high pollutant removal efficiency. Furthermore, the ability of light to regenerate iron oxides enables the reaction to proceed effectively in the presence of mining waste, regardless of the oxidation state of iron.

Hollanda *et al.* synthesized a catalyst from amethyst mining reject, utilizing ball milling to reduce and homogenize its size, thereby increasing its surface area.[44] In the pollutant removal experiment, a 96.5% removal efficiency was achieved using 0.75 g L^{-1} of catalyst, enhanced by the Fe^{2+}/Fe^{3+} redox cycle under visible light (entry 5, Table 8).[44] In the fourth cycle, 92.8% phenol degradation was achieved, demonstrating high

stability and catalytic activity, with iron leaching (1.23 mg L^{-1}) remaining well below the Brazilian regulatory limit of 15 mg L^{-1}.[120] da Silva *et al.*[114] and Rojas-Mantilla *et al.*[115] utilized ilmenite mining residue and iron mining residue as catalysts without additional modification. Despite its lower specific surface area than other catalysts,[37] the ilmenite residue exhibited excellent pollutant removal efficiency, achieving 89% for sulfamethoxazole, 83% for ciprofloxacin, and 88% for tetracycline with 0.277 g L^{-1} of catalyst (entry 6, Table 8). Meanwhile, the iron mining residue-based catalyst achieved a 96% decomposition rate for sulfathiazole at a catalyst dose of 0.3 g L^{-1} (entry 7, Table 8). While both catalysts operated under UVA conditions, the iron mining residue, with a specific surface area more than four times higher, promoted greater radical generation, leading to an increased decomposition rate. Furthermore, the iron mining residue catalyst exhibited an electrical energy consumption of 1.3 kW h m^{-3} due to its rapid decomposition performance, highlighting its lower energy demands compared to other catalysts reported in the literature. When Kebir *et al.* calcined iron mining waste at 500 °C, the modified catalyst exhibited enhanced catalytic activity by increasing the active surface area and optimizing the distribution of active sites.[112] Using 0.15 g L^{-1} of catalyst at pH 3 and 0.45 mM Na_2SO_3 under sunlight for 90 min, a dye removal rate of 91.5% was achieved (entry 8, Table 8). Despite Na_2SO_3 acting as an oxidizing agent, OH• and $O_2^{•-}$ radicals were generated through catalytic activation by light, with $OH^•$ radicals playing a dominant role in pollutant decomposition. Drumm *et al.* assessed the catalytic performance of basalt mine tailings sieved to a uniform size without additional modification.[47] In dye removal experiments, the catalyst achieved 97% pollutant removal efficiency and a total organic carbon removal rate of 75.4% after 300 min (entry 9, Table 8). Light-reduced Fe^{2+} reacted with H_2O_2 to produce OH• radicals, which rapidly decomposed pollutants and efficiently mineralized them into CO_2 and H_2O. Fig. 6 indicates that the photo-Fenton process, like the traditional Fenton process, is more effective under low pH conditions. However, the photoreduction of Fe^{3+} to Fe^{2+} enhances the generation of OH•, thereby further accelerating the pollutant degradation rate.

5.4. PMS activation

Unlike the traditional Fenton process, the PMS activation process utilizes PMS as an oxidizing agent, generating $SO_4^{•-}$ radicals, $O_2^{•-}$ radicals, and $^1O_2$ as the primary reactive oxygen species for pollutant decomposition. In this process, various metals, including Fe, can participate, and PMS activation may also occur through carbon bonding.[121] A detailed analysis was conducted to examine the active sites and radical generation involved in the PMS activation process.

Wang *et al.* developed a PMS activation catalyst with waste ore and fine needle powder, mixed in a specific ratio and calcined at 600 °C to produce a metal composite-loaded biochar.[33] Co^{2+}, Fe^{2+}, Co^{3+}, and Fe^{3+} coexisted in the catalyst, actively contributing to the PMS activation reaction, as evidenced by the reduction in peak intensities. Under optimal
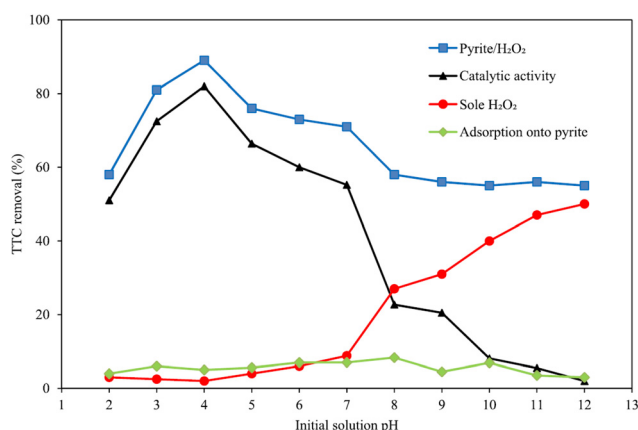

Fig. 5 Effect of pH on pollutant removal efficiency in the Fenton process. Reprinted from Mashayekh-Salehi *et al.*,[113] copyright (2020), with permission from Elsevier.
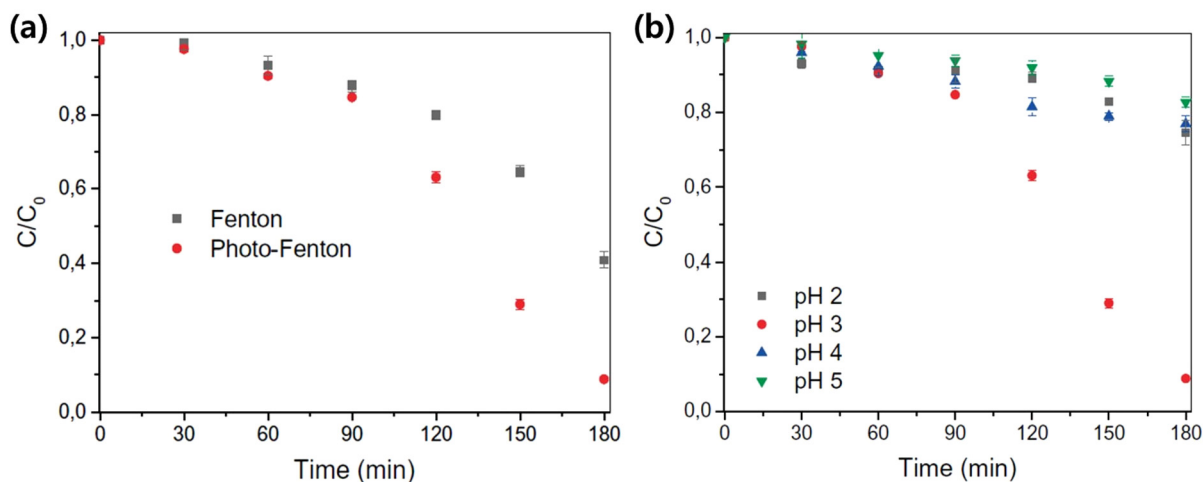
Fig. 6 (a) Comparison of catalytic activities on pollutant removal and the effect of pH on the photo-Fenton process. Reprinted from Hollanda *et al.*,[44] copyright (2024), with permission from Springer Nature.

reaction conditions, the catalyst degraded 96.6% of tetracycline within 60 min (entry 10, Table 8). PMS was decomposed by metal oxidation to form $SO_4^{\bullet-}$ radicals and $OH\bullet$ radicals, but $SO_4^{\bullet-}$ radicals mainly had a major influence on the decomposition of pollutants. Bicalho *et al.*[38] and Zhang *et al.*[58] synthesized catalysts by combining iron mining waste and coal gangue with graphitic carbon nitride. During the calcination process for graphitic carbon nitride synthesis, iron mining waste and metal gangue were incorporated in specific ratios, resulting in catalysts with various metal oxides distributed across the carbon nitride layer. The metals, dispersed over a large specific surface area, contributed to PMS activation for radical generation, while electron transfer at defect sites in carbon nitride further facilitated PMS activation. The iron mining waste-based catalyst achieved 98% acetaminophen removal efficiency (entry 11, Table 8), while the coal gangue-based catalyst demonstrated 90% bisphenol A removal efficiency (entry 12, Table 8). In both catalysts, various reactive oxygen species, including $SO_4^{\bullet-}$ and $OH\bullet$ radicals, were generated; however, $^1O_2$ and $O_2^{\bullet-}$ radicals played a more significant role in pollutant decomposition. This suggests that the formation of $O_2^{\bullet-}$ and $^1O_2$ species was enhanced by the electron-deficient environment created due to differences in electronegativity.[122]

5.5. Electrochemical treatment

In the electrochemical process, the power generation capacity is influenced by anode characteristics such as potential and surface modification. Increased power generation enhances process efficiency while reducing energy consumption.[123] With high chemical stability, mechanical strength, porosity, and specific surface area, mining waste serves as a cost-effective material that significantly boosts efficiency. Eslami *et al.* synthesized anode electrodes using pumice mining waste and applied them to electrochemical processes.[50] The pumice was standardized in size through crushing and milling operations

before being coated onto carbon cloth. A binder was added to secure the coating, and the assembly was calcined at 160 °C. With its high specific surface area, the pumice-coated electrode enhanced the adsorption of electrically generated microorganisms compared to uncoated electrodes. It also accelerated electron accumulation, resulting in a 47% increase at open circuit voltage. This electrode modification significantly improved the efficiency of COD decomposition in water, achieving over 40% improvement, with COD removal reaching 94% (entry 13, Table 8). Additionally, removal efficiencies for total suspended solids and total dissolved solids ranged from 70% to 80%. These improvements were attributed to enhanced electron transfer due to the accumulation of electrons in the electrode.[124] Notably, the study, conducted with actual wastewater, demonstrated an energy efficiency improvement of 32%.

5.6. Ozonation

The ozone process primarily focuses on evaluating the extent to which O_3 decomposition is enhanced by the catalyst. In this process, the metal oxides present in the mining waste catalyst play a crucial role by promoting more efficient ion exchange and radical formation.[39] This, in turn, leads to a significant increase in the ozone decomposition rate, enhancing the overall effectiveness of the process. Gier Della Rocca *et al.* synthesized an ozone generation catalyst using magnetic mining waste and investigated its application in pollutant decomposition *via* ozone oxidation.[39,40] Magnetic mining waste was mixed with alkali activators (Na_2SiO_3, NaOH, and H_2O) in specific ratios and reacted for 15 min at 65 °C to produce an inorganic binder, *i.e.*, a geopolymer. Metakaolin, synthesized by calcining kaolin (Campina Grande, PB, Brazil), served as a control. Results revealed that the surface area of the catalyst decreased as the waste ratio increased. However, the catalytic performance improved, with the ozone decomposition rate peaking at waste ratios of 25–50 wt% (entry 14, Table 8). The application of the synthetic catalyst resulted in a 60% ozone

decomposition rate and a 71% pollutant removal efficiency (entry 15, Table 8). Furthermore, mineralization, which was only 4% without the catalyst, increased significantly to 40% with its application.

6. Summary and outlook

This review evaluated the performance of mining waste-derived catalysts across diverse fields of application. The catalytic properties of mining waste were examined in relation to their treatment procedures, highlighting their significant potential in various processes, including reforming, wastewater treatment, esterification, and environmental catalysis (e.g., denitrification, CO oxidation, and CO_2 reduction). These findings demonstrate that mining waste can effectively replace costly and non-renewable conventional catalysts in several applications. Despite these promising results, there is still a need to further investigate the design of optimal mining waste-derived catalysts with enhanced activity and stability for different reactions. Continuous efforts in this field will not only improve the management of mining waste but also promote the sustainability of catalytic processes. To this end, several points need to be considered in future studies for further enhancement of the feasibility of mining waste-derived catalysts.

First, various types of mining waste have been employed as heterogeneous catalysts, with characteristics such as composition, crystallite size (e.g., spinel), and impurities differing significantly based on their origin. However, inconsistencies in the characterization methods used across studies present a major challenge. For example, one study may report the content of metals measured via X-ray fluorescence, while another reports the content of metal oxides estimated via X-ray diffraction. These variations hinder the direct comparison of findings and complicate efforts to design more active and selective catalysts for specific reactions. Standardizing characterization techniques for mining waste is, therefore, essential to ensure uniformity and reproducibility in future research.

To enhance the catalytic properties of mining waste-derived catalysts—such as the type and number of active sites, surface area, porosity, and surface-active site density—greater efforts are needed to control the combined effects of key variables, including the type of mining waste and catalyst preparation conditions. However, little information is available on precise control over mining waste properties for catalytic applications. Further investigation into tailoring these properties is essential for designing active, selective, and stable mining waste-derived catalysts.

Although a few studies have reported data on equilibrium and kinetics for a limited range of reactions (e.g., reforming) conducted on mining waste-derived catalysts, more comprehensive studies are needed. Detailed investigations into chemical equilibrium, reaction kinetics, and thermodynamics for a broader array of reactions occurring over mining waste-derived catalysts are essential. These studies should also assess catalytic performance factors such as reaction rates, selectivity toward target products, and the extent of catalyst deactivation after reactions. This information is critical for process intensification and scaling up mining waste-based catalytic processes.

Various mining wastes have been modified and utilized as catalysts for wastewater treatment, demonstrating excellent pollutant removal performance. However, the range of pollutant types tested with these catalysts remains narrow, and their applicability to actual wastewater conditions is underexplored. Many studies lack comprehensive analyses of changes in catalyst performance when key parameters (e.g., temperature, scavengers, and anions) or water matrices (e.g., natural organic matter) are varied. These gaps make it challenging to evaluate the practicality and scalability of mining waste-derived catalysts in real-world applications. To address these issues, future research should focus on expanding the evaluation of these catalysts to include a broader spectrum of pollutants and perform correlation analyses with additional influencing factors.

In the studies reviewed, catalyst performance was primarily evaluated under controlled conditions using a single water treatment process, often achieving a removal efficiency of approximately 90%. While this performance is excellent, the presence of co-existing materials and background compounds in actual wastewater may significantly reduce the removal efficiency. To improve the practical applicability of mining waste-derived catalysts, further research should focus on optimizing catalyst performance through advanced reforming methods or by integrating multiple water treatment processes.

While mining waste-derived catalysts have shown great promise in various reactions, it is difficult to designate optimal reaction conditions for each of them because different studies have used different reaction conditions (e.g., temperature, pressure, time-on-stream, and more importantly, space velocity). Moreover, their stability and durability during long-term operations remain uncertain. Catalyst deactivation, particularly under high-temperature and high-pressure conditions, poses a significant challenge. Rigorous studies are required to optimize the reactions of mining waste catalysts and enhance the stability and durability of these catalysts, ensuring their ability to support continuous operations without significant performance degradation.

For mining waste to become a viable substitute for industrial catalysts, a stable and consistent supply of raw mining waste and residue is essential. Maintaining constant properties for large-scale catalyst production is critical for achieving industrial applicability. Addressing this challenge will require close cooperation between the chemical and mining industries, as well as local governments. To promote the integration of mining waste into catalyst production, tools such as techno-economic analysis (TEA) and life cycle assessment (LCA) should be employed. These methods can simulate the real-world application of mining waste-derived catalysts and highlight their contribution to sustainable mining waste management by demonstrating their potential to replace expensive and non-environmentally benign catalysts.

Data availability

No primary research results, software or code have been included and no new data were generated or analysed as part of this review.

Conflicts of interest

There are no conflicts to declare.

Acknowledgements

References

1 O. Agboola, D. E. Babatunde, O. S. I. Fayomi, E. R. Sadiku, P. Popoola, L. Moropeng, A. Yahaya and O. A. Mamudu, *Results Eng.*, 2020, **8**, 100181.

2 J. Helser, E. Vassilieva and V. Cappuyns, *J. Hazard. Mater.*, 2022, **424**, 127313.

3 W. Haas, F. Krausmann, D. Wiedenhofer and M. Heinz, *J. Ind. Ecol.*, 2015, **19**, 765–777.

4 D. M. Franks, M. Stringer, L. A. Torres-Cruz, E. Baker, R. Valenta, K. Thygesen, A. Matthews, J. Howchin and S. Barrie, *Sci. Rep.*, 2021, **11**, 5353.

5 *Mining waste management market size, share & industry analysis, by source (surface mining and underground mining), by waste type (solid waste {waste rock, tailings, others} and liquid waste), by commodity (mineral fuels, iron, ferro alloys, industrial minerals, and others) and regional forecast, 2024–2032*, Fortune Business Insights, Pune, Maharashtra, India, 2024.

6 D. A. Vallero and G. Blight, Mine waste: a brief overview of origins, quantities, and methods of storage, in *Waste*, ed. T. M. Letcher and D. A. Vallero, Academic Press, Cambridge, MA, USA, 2nd edn, 2019, pp. 129–151, DOI: **10.1016/B978-0-12-815060-3.00006-2**.

7 S. Kalisz, K. Kibort, J. Mioduska, M. Lieder and A. Małachowska, *J. Environ. Manage.*, 2022, **304**, 114239.

8 L. N. Bowker and D. M. Chambers, *Earthwork Act*, 2015, **24**, 1–56.

9 R. K. Valenta, É. Lèbre, C. Antonio, D. M. Franks, V. Jokovic, S. Micklethwaite, A. Parbhakar-Fox, K. Runge, E. Savinova, J. Segura-Salazar, M. Stringer, I. Verster and M. Yahyaei, *Resour., Conserv. Recycl.*, 2023, **190**, 106859.

10 P. Segui, A. e. M. Safhi, M. Amrani and M. Benzaazoua, *Minerals*, 2023, **13**, 90.

11 S. Maruthupandian, A. Chaliasou and A. Kanellopoulos, *Constr. Build. Mater.*, 2021, **312**, 125333.

12 Z. Mkahal, Y. Mamindy-Pajany, W. Maherzii and N.-E. Abriak, *Waste Biomass Valorization*, 2022, **13**, 667–687.

13 S. Yagüe, I. Sánchez, R. Vigil de la Villa, R. García-Giménez, A. Zapardiel and M. Frías, *Minerals*, 2018, **8**, 46.

14 Y. W. Choi, Y. J. Kim, O. Choi, K. M. Lee and M. Lachemi, *Constr. Build. Mater.*, 2009, **23**, 2481–2486.

15 A. M. T. Simonsen, S. Solismaa, H. K. Hansen and P. E. Jensen, *Waste Manage.*, 2020, **102**, 710–721.

16 S. Maruthupandian, *Upcycling mineral wastes: their characterisation and activation for use in sustainable cementitious binders*, University of Hertfordshire, 2024, DOI: **10.18745/th.28078**.

17 I. Capasso, S. Lirer, A. Flora, C. Ferone, R. Cioffi, D. Caputo and B. Liguori, *J. Cleaner Prod.*, 2019, **220**, 65–73.

18 S. M. A. Qaidi, B. A. Tayeh, A. M. Zeyad, A. R. G. de Azevedo, H. U. Ahmed and W. Emad, *Case Stud. Constr. Mater.*, 2022, **16**, e00933.

19 G. Lazorenko, A. Kasprzhitskii, F. Shaikh, R. S. Krishna and J. Mishra, *Process Saf. Environ. Prot.*, 2021, **147**, 559–577.

20 X. He, Z. Yuhua, S. Qaidi, H. F. Isleem, O. Zaid, F. Althoey and J. Ahmad, *Ceram. Int.*, 2022, **48**, 24192–24212.

21 L. D. Menéndez-Aguado, M. Marina Sánchez, M. A. Rodríguez, A. L. Coello Velázquez and J. M. Menéndez-Aguado, *Materials*, 2019, **12**, 2047.

22 A. J. Whitworth, E. Forbes, I. Verster, V. Jokovic, B. Awatey and A. Parbhakar-Fox, *Cleaner Eng. Technol.*, 2022, **7**, 100451.

23 C. Falagán, B. M. Grail and D. B. Johnson, *Miner. Eng.*, 2017, **106**, 71–78.

24 B. Lim and R. D. Alorro, *Sustainable Chem.*, 2021, **2**, 686–706.

25 C. Vitti and B. J. Arnold, *Min., Metall., Explor.*, 2022, **39**, 49–54.

26 S. K. Sarker, N. Haque, M. Bhuiyan, W. Bruckard and B. K. Pramanik, *J. Environ. Chem. Eng.*, 2022, **10**, 107622.

27 A. Abbadi and G. Mucsi, *J. Environ. Chem. Eng.*, 2024, **12**, 113118.

28 Z. Xiaolong, Z. Shiyu, L. Hui and Z. Yingliang, *J. Cleaner Prod.*, 2021, **284**, 124756.

29 O. R. Carmignano, S. S. Vieira, A. P. C. Teixeira, F. S. Lameiras, P. R. G. Brandão and R. M. Lago, *J. Braz. Chem. Soc.*, 2021, **32**, 1895–1911.

30 F. P. Barraza, D. Thiyagarajan, A. Ramadoss, V. S. Manikandan, S. S. Dhanabalan, C. V. Abarzúa, P. S. Soloaga, J. C. Nazer, M. J. Morel and A. Thirumurugan, *Renewable Sustainable Energy Rev.*, 2024, **202**, 114665.

31 V. Maus, S. Giljum, D. M. da Silva, J. Gutschlhofer, R. P. da Rosa, S. Luckeneder, S. L. B. Gass, M. Lieber and I. McCallum, *Sci. Data*, 2022, **9**, 433.

32 M. Jayakumar, U. Surendran, P. Raja, A. Kumar and V. Senapathi, *Arabian J. Geosci.*, 2021, **14**, 2156.

33 J. Wang, N. Huang, G. Wang, J. Yu, F. Wang, D. Zhang, F. Su, X. Jia, M. Wang, X. Meng, C. Kong, Z. Yang, T. Wang and H. Zhu, *Colloids Surf., A*, 2024, **685**, 133249.

34 A. Azara, E.-H. Benyoussef, F. Mohellebi, M. Chamoumi, F. Gitzhofer and N. Abatzoglou, *Catalysts*, 2019, **9**, 1069.

35 C. D. Prates, F. C. Ballotin, H. Limborço, J. D. Ardisson, R. M. Lago and A. P. d. C. Teixeira, *Appl. Catal., A*, 2020, **600**, 117624.

36 T. d. M. Augusto, P. Chagas, D. L. Sangiorge, T. C. d. O. M. Leod, L. C. A. Oliveira and C. S. d. Castro, *J. Environ. Chem. Eng.*, 2018, **6**, 6545–6553.

37 S. C. Ayala-Durán, P. Hammer and R. F. P. Nogueira, *Environ. Sci. Pollut. Res.*, 2020, **27**, 1710–1720.

38 H. A. Bicalho, R. D. F. Rios, I. Binatti, J. D. Ardisson, A. J. Howarth, R. M. Lago and A. P. C. Teixeira, *J. Hazard. Mater.*, 2020, **400**, 123310.

39 D. G. D. Rocca, F. A. S. e Sousa, J. D. Ardisson, R. A. Peralta, E. Rodríguez-Castellón and R. d. F. P. M. Moreira, *Heliyon*, 2023, **9**, e17097.

40 D. G. Della Rocca, A. De Noni Júnior, E. Rodríguez-Aguado, R. A. Peralta, E. Rodríguez-Castellón, G. L. Puma and R. F. P. M. Moreira, *J. Environ. Chem. Eng.*, 2023, **11**, 111163.

41 M. Mpiliou, K. Kappis, S. Tombros, G. Avgouropoulos, S. Kokkalas, P. Lampropoulou, S. Triantafyllidis, H. Li and J. Papavasiliou, *Sustainable Chem. Environ.*, 2024, **5**, 100067.

42 S. Belbessai, E.-H. Benyoussef, F. Gitzhofer and N. Abatzoglou, *Chem. Eng. J. Adv.*, 2022, **12**, 100424.

43 M. Chamoumi and N. Abatzoglou, *Catalysts*, 2021, **11**, 771.

44 L. R. Hollanda, J. A. B. de Souza, G. L. Dotto, E. L. Foletto and O. Chiavone-Filho, *Environ. Sci. Pollut. Res.*, 2024, **31**, 21291–21301.

45 E. Karimi, I. F. Teixeira, L. P. Ribeiro, A. Gomez, R. M. Lago, G. Penner, S. W. Kycia and M. Schlaf, *Catal. Today*, 2012, **190**, 73–88.

46 E. D. A. Santosa, M. Tamyiz, S. Sagadevan, A. Hidayat, I. Fatimah and R.-a. Doong, *Results Chem.*, 2022, **4**, 100451.

47 F. C. Drumm, P. Grassi, J. Georgin, D. P. Franco, D. Tonato, E. L. Foletto, G. L. Dotto and S. L. Jahn, *Appl. Geochem.*, 2022, **136**, 105136.

48 M. Chamoumi, N. Abatzoglou, J. Blanchard, M.-C. Iliuta and F. Larachi, *Catal. Today*, 2017, **291**, 86–98.

49 M. A. P. Cechinel, T. de Oliveira Guidolin, A. R. da Silveira, J. dos Santos Tasca, O. R. K. Montedo and S. Arcaro, *Sci. Total Environ.*, 2022, **807**, 150823.

50 F. Eslami, K. Yaghmaeian, R. Shokoohi, R. Sajjadipoya, A. Rahmani, H. Askarpur, A. N. Baghani, H. J. Mansoorian and F. j. Ansari, *Heliyon*, 2024, **10**, e40495.

51 Z. Wang, Y. Huang, H. Luo, Z. Gong, K. Zhang, N. Li and W. Wu, *Green Process. Synth.*, 2019, **8**, 865–872.

52 J. Wang, C. Zhu, B. Li, Z. Gong, Z. Meng, G. Xu and W. Wu, *Green Process. Synth.*, 2020, **9**, 191–202.

53 L. Hou, Z. Li, J. Xu and W. Wu, *React. Kinet., Mech. Catal.*, 2023, **136**, 2499–2516.

54 E. T. L. Lima, L. S. Queiroz, L. H. de Oliveira Pires, R. S. Angélica, C. E. F. da Costa, J. R. Zamian, G. N. da Rocha Filho, R. Luque and L. A. S. d. Nascimento, *ACS Sustainable Chem. Eng.*, 2019, **7**, 7543–7551.

55 A. d. N. de Oliveira, E. T. L. Lima, E. H. de Aguiar Andrade, J. R. Zamian, G. N. d. R. Filho, C. E. F. d. Costa, L. H. de Oliveira Pires, R. Luque and L. A. S. d. Nascimento, *Catalysts*, 2020, **10**, 478.

56 Y. Zhang, W. Ma, Z. Zhang, Y. Chen, J. Sun, S. Yue, G. Wang and X. Wang, *J. Environ. Manage.*, 2025, **373**, 123557.

57 S. Bahraminia and M. Anbia, *Int. J. Hydrogen Energy*, 2024, **83**, 842–855.

58 X. Zhang, R. Zhao, N. Zhang, Y. Su, Z. Liu, R. Gao and C. Du, *Appl. Catal., B*, 2020, **263**, 118316.

59 É. Lèbre, G. D. Corder and A. Golev, *Miner. Eng.*, 2017, **107**, 34–42.

60 R. Zhang, H. He, Y. Tang, Z. Zhang, H. Zhou, J. Yu, L. Zhang and B. Dai, *ChemCatChem*, 2024, **16**, e202400396.

61 H. Lee, Y. Kim, H. K. Yu and J. Lee, *Alexandria Eng. J.*, 2024, **91**, 494–502.

62 W. Yang, D. Choi, H. K. Yu, S. Jung and J. Lee, *J. Environ. Manage.*, 2025, **373**, 123564.

63 W. Yang, S. Jung, J. Lee, S. W. Lee, Y. T. Kim and E. E. Kwon, *Environ. Pollut.*, 2023, **329**, 121684.

64 H. S. Lee, S. Jung, S. W. Lee, Y. T. Kim and J. Lee, *Korean J. Chem. Eng.*, 2023, **40**, 2472–2479.

65 I. Riaz, O. A. Qamar, F. Jamil, M. Hussain, A. Inayat, L. Rocha-Meneses, P. Akhter, S. Musaddiq, M. R. A. Karim and Y. Park, *Korean J. Chem. Eng.*, 2023, **40**, 2683–2691.

66 I. Boz, M. S. Boroglu, Y. Zengin and B. Kaya, *Korean J. Chem. Eng.*, 2023, **40**, 1882–1891.

67 O. B. Al-Ameri, M. Alzuhairi, E. Bailón-García, F. Carrasco-Marín and J. Amaro-Gahete, *Appl. Sci.*, 2024, **14**, 9080.

68 Hartati, D. Prasetyoko, M. Santoso, I. Qoniah, W. L. Leaw, P. B. D. Firda and H. Nur, *J. Chin. Chem. Soc.*, 2020, **67**, 911–936.

69 É. Ujaczki, V. Feigl, M. Molnár, P. Cusack, T. Curtin, R. Courtney, L. O'Donoghue, P. Davris, C. Hugi, M. W. Evangelou, E. Balomenos and M. Lenz, *J. Chem. Technol. Biotechnol.*, 2018, **93**, 2498–2510.

70 M. I. Malik, M. Rouabah, N. Abatzoglou and I. E. Achouri, *Biofuels, Bioprod. Biorefin.*, 2024, **18**, 1027–1046.

71 S. Belbessai, I. E. Achouri, E. H. Benyoussef, F. Gitzhofer and N. Abatzoglou, *Catal. Today*, 2021, **365**, 111–121.

72 O. A. Z. Sahraei, F. Larachi, N. Abatzoglou and M. C. Iliuta, *Appl. Catal., B*, 2017, **219**, 183–193.

73 O. A. Sahraei, A. Desgagnés, F. Larachi and M. C. Iliuta, *Appl. Catal., B*, 2020, **279**, 119330.

74 O. A. Sahraei, A. Desgagnés, F. Larachi and M. C. Iliuta, *Int. J. Hydrogen Energy*, 2021, **46**, 32017–32035.

75 M. Farsi, Ammonia production from syngas: plant design and simulation, in *Advances in Synthesis Gas: Methods, Technologies and Applications*, ed. M. R. Rahimpour, M. A. Makarem and M. Meshksar, Elsevier, Amsterdam, Netherlands, 2023, vol. 4, pp. 381–399.

76 S. Sepahi and M. R. Rahimpour, Methanol production from syngas, in *Advances in Synthesis Gas : Methods, Technologies and Applications*, ed. M. R. Rahimpour,

M. A. Makarem and M. Meshksar, Elsevier, Amsterdam, Netherlands, 2023, vol. 3, pp. 111–146.

77 S. Lee, J.-C. Seo, H.-J. Chun, S. Yang, E.-h. Sim, J. Lee and Y. T. Kim, *Catal. Sci. Technol.*, 2022, **12**, 5814–5828.

78 J. Lee, K.-Y. A. Lin, S. Jung and E. E. Kwon, *Chem. Eng. J.*, 2023, **452**, 139218.

79 J. Lee, S. Kim, S. You and Y.-K. Park, *Renewable Sustainable Energy Rev.*, 2023, **178**, 113240.

80 V. A. Luciano, F. G. de Paula, P. S. Pinto, C. D. Prates, R. C. G. Pereira, J. D. Ardisson, M. G. Rosmaninho and A. P. C. Teixeira, *Fuel*, 2022, **310**, 122290.

81 E. Benhelal, M. Hoseinpour, R. Karami, A. Mirvakili and M. I. Rashid, Energy and exergy analysis of blue hydrogen production and conversion, in *Hydrogen Energy Conversion and Management*, ed. M. M. K. Khan, A. K. Azad and A. M. T. Oo, Elsevier, Amsterdam, Netherlands, 2024, pp. 157–207, DOI: 10.1016/B978-0-443-15329-7.00008-9.

82 H. Zhu, H. Chen, M. Zhang, C. Liang and L. Duan, *Catal. Sci. Technol.*, 2024, **14**, 1712–1729.

83 S. Wang, Z. Shen, A. Osatiashtiani, S. A. Nabavi and P. T. Clough, *Chem. Eng. J.*, 2024, **486**, 150170.

84 H. S. Bengaard, J. K. Nørskov, J. Sehested, B. S. Clausen, L. P. Nielsen, A. M. Molenbroek and J. R. Rostrup-Nielsen, *J. Catal.*, 2002, **209**, 365–384.

85 L. a. Garcia, R. French, S. Czernik and E. Chornet, *Appl. Catal., A*, 2000, **201**, 225–239.

86 S. Mushtaq, J. Lee, F. Jamil, S. Imran, P. Akhter, M. Hussain and Y.-K. Park, *Energy Environ.*, 2025, **36**, 1063–1079.

87 J. E. Lee, J. Lee, H. Jeong, Y.-K. Park and B.-S. Kim, *Chem. Eng. J.*, 2023, **475**, 146108.

88 A. Desgagnés and M. C. Iliuta, *Chem. Eng. J.*, 2022, **429**, 132278.

89 C. Ratnasamy and J. P. Wagner, *Catal. Rev.*, 2009, **51**, 325–440.

90 A. Boudjemaa, C. Daniel, C. Mirodatos, M. Trari, A. Auroux and R. Bouarab, *C. R. Chim.*, 2011, **14**, 534–538.

91 L. Chen, C. K. S. Choong, Z. Zhong, L. Huang, T. P. Ang, L. Hong and J. Lin, *J. Catal.*, 2010, **276**, 197–200.

92 D. G. Rethwisch and J. A. Dumesic, *Appl. Catal.*, 1986, **21**, 97–109.

93 A. d. N. de Oliveira, I. M. Ferreira, D. E. Q. Jimenez, L. S. da Silva, A. A. F. da Costa, E. T. L. Lima, F. F. Costa, P. T. S. da Luz, G. N. d. R. Filho, S. M. Osman, R. Luque and L. A. S. d. Nascimento, *Mol. Catal.*, 2022, **528**, 112504.

94 J.-H. Kim, M. Kim, G. Park, E. Kim, H. Song, S. Jung, Y.-K. Park, Y. F. Tsang, J. Lee and E. E. Kwon, *Biotechnol. Adv.*, 2024, **75**, 108418.

95 D.-W. Lee and K.-Y. Lee, *Catal. Surv. Asia*, 2014, **18**, 55–74.

96 S. Valizadeh, B. Valizadeh, J. Lee and Y.-K. Park, *ChemCatChem*, 2025, **17**, e202401390.

97 S. Kim, E. E. Kwon, Y. T. Kim, S. Jung, H. J. Kim, G. W. Huber and J. Lee, *Green Chem.*, 2019, **21**, 3715–3743.

98 P. Brimblecombe, M. Chu, C.-H. Liu, Y. Fu, P. Wei and Z. Ning, *Atmos. Environ.*, 2023, **295**, 119562.

99 S. Bhowmick, A. Badiwal and K. T. Shenoy, *Chem. Eng. J. Adv.*, 2023, **15**, 100511.

100 Y.-K. Park and B.-S. Kim, *Chem. Eng. J.*, 2023, **461**, 141958.

101 G. Li, B. Wang, H. Wang, J. Ma, W. Q. Xu, Y. Li, Y. Han and Q. Sun, *Catal. Commun.*, 2018, **108**, 82–87.

102 S. Xie, Y. Lu, K. Ye, W. Tan, S. Cao, C. Wang, D. Kim, X. Zhang, J. Loukusa, Y. Li, Y. Zhang, L. Ma, S. N. Ehrlich, N. S. Marinkovic, J. Deng, M. Flytzani-Stephanopoulos and F. Liu, *Environ. Sci. Technol.*, 2024, **58**, 12731–12741.

103 Q. Jiang, J. Zhang, H. Huang, Y. Wu and Z. Ao, *J. Mater. Chem. A*, 2020, **8**, 287–295.

104 S. Dey and G. C. Dhal, *Mater. Sci. Energy Technol.*, 2020, **3**, 6–24.

105 S. Y. Lim, S. A. Younis, K.-H. Kim and J. Lee, *Chem. Soc. Rev.*, 2024, **53**, 9976–10011.

106 A. Modak, P. Bhanja, S. Dutta, B. Chowdhury and A. Bhaumik, *Green Chem.*, 2020, **22**, 4002–4033.

107 N. Czuma, K. Zarębska, M. Motak, M. E. Gálvez and P. Da Costa, *Fuel*, 2020, **267**, 117139.

108 F. Rahimi, J. P. van der Hoek, S. Royer, A. Javid, A. Mashayekh-Salehi and M. J. Sani, *J. Water Process Eng.*, 2021, **40**, 101808.

109 X. Guo, M. Zeng, H. Yu, F. Lin, J. Li, W. Wang and G. Chen, *J. Cleaner Prod.*, 2024, **459**, 142457.

110 J. Zhou, X. Ren, Z. Liu and S. Yuan, *Mater. Today Sustainability*, 2022, **20**, 100225.

111 C. M. Oliveira, C. M. Machado, G. W. Duarte and M. Peterson, *J. Cleaner Prod.*, 2016, **139**, 821–827.

112 M. Kebir, H. Tahraoui, I. K. Benramdane, N. Nasrallah, S. Toumi, J. Zhang and A. Amrane, *Water Resour. Ind.*, 2024, **32**, 100269.

113 A. Mashayekh-Salehi, K. Akbarmojeni, A. Roudbari, J. Peter van der Hoek, R. Nabizadeh, M. H. Dehghani and K. Yaghmaeian, *J. Cleaner Prod.*, 2021, **291**, 125235.

114 M. R. da Silva, D. L. Cunha, A. Kuznetsov, J. R. Araujo, A. Della-Flora, A. Dallegrave, C. Sirtori and E. M. Saggioro, *J. Environ. Chem. Eng.*, 2024, **12**, 111844.

115 H. D. Rojas-Mantilla, S. C. Ayala-Durán and R. F. P. Nogueira, *J. Environ. Sci. Health, Part A*, 2019, **54**, 1277–1286.

116 F. Deng, H. Olvera-Vargas, M. Zhou, S. Qiu, I. Sirés and E. Brillas, *Chem. Rev.*, 2023, **123**, 4635–4662.

117 F. Cai, C. Sun, Z. Sun, Y. Lai and H. Ding, *Appl. Surf. Sci.*, 2023, **623**, 157044.

118 V. V. Figueiredo, R. P. F. Bonfim, M. A. Silva, C. R. Moreira, G. A. C. Pérez, W. A. Lourenço, B. R. Salles and V. M. M. Salim, *Mater. Chem. Phys.*, 2025, **337**, 130564.

119 H. Yang, S.-H. Jung, J. H. Lee, I. S. Cho, S.-J. Park and C.-G. Lee, *J. Water Process Eng.*, 2024, **68**, 106411.

120 J. C. Mathews, F. P. da Costa Assunção, D. O. Pereira, J. C. C. da Silva, F. F. S. Almeida, A. C. P. Almeida, N. M. Mendonça, I. W. de Sousa Brandão, A. O. Menezes, L. E. P. Borges, J. F. H. Ferreira, J. A. R. Pereira and N. T. Machado, *Sustainability*, 2024, **16**, 8370.

121 H. Yang, C.-G. Lee and J. Lee, *J. Water Process Eng.*, 2023, **56**, 104545.

122 W.-D. Oh, A. Veksha, X. Chen, R. Adnan, J.-W. Lim, K.-H. Leong and T.-T. Lim, *Chem. Eng. J.*, 2019, **374**, 947–957.

123 Y. Liu, Y. Sun, M. Zhang, S. Guo, Z. Su, T. Ren and C. Li, *J. Colloid Interface Sci.*, 2023, **629**, 970–979.

124 J. S. Santos, M. Tarek, M. S. Sikora, S. Praserthdam and P. Praserthdam, *J. Power Sources*, 2023, **564**, 232872.